Desalination and Water Treatment
www.deswater.com

doi: 10.5004/dwt.2017.21691

97 (2017) 338–362
November

Optimization, kinetics, equilibrium isotherms, and thermodynamics studies for Congo red dye adsorption using calcium alginate beads immobilized with dual adsorbent (*Neurospora crassa* dead fungal biomass and wheat bran)

P. Vairavel[a], V. Ramachandra Murty[b,*]

[a]*Department of Chemical Engineering, Manipal Institute of Technology, Manipal Academy of Higher Education, Manipal, Karnataka, India, Tel. +91 9036270978; email: pvairavel@gmail.com*
[b]*Department of Biotechnology, Manipal Institute of Technology, Manipal Academy of Higher Education, Manipal, Karnataka, India, Tel. +91 9448529691; emails: vytlarama@yahoo.com, murty.vytla@manipal.edu*

Received 26 June 2017; Accepted 17 November 2017

ABSTRACT

The present study is concerned with the batch adsorption of Congo red (CR) from aqueous solutions using calcium alginate beads (CAB) immobilized with dead biomass of *Neurospora crassa* along with wheat bran (DB–WB) as a dual adsorbent. The optimum conditions for CR adsorption were determined by studying various operational parameters such as initial pH, dye concentration, dual adsorbent loading in CAB, adsorbent dosage, agitation speed, and temperature. The process parameters were optimized using factorial experimental design to attain the maximum percentage adsorption. The CAB immobilized with DB–WB was characterized by attenuated transmission reflector and field emission scanning electron microscopy/energy dispersive X-ray spectroscopy (FESEM/EDS) analysis. The experimental equilibrium data were analyzed with various isotherm models. The results show that the best fit was achieved with the Langmuir isotherm model. Kinetic rate constants were found using different kinetic models. The adsorption kinetics for CR dye removal by CAB immobilized with DB–WB dual adsorbent follows pseudo-second-order kinetic model. Thermodynamic studies were performed to determine the change in Gibbs free energy (ΔG), change in enthalpy (ΔH), and change in entropy (ΔS) of the adsorption process. Thermodynamic parameters were evaluated by maximum adsorption capacities (q_{max}) at different temperatures. From the results, the adsorption was found to be spontaneous, endothermic in nature of the adsorption process and favored at high temperature. Desorption experiments were carried out using various desorbing agents to explore the possibility of regenerating the CAB immobilized with dual adsorbent. The maximum percentage of CR dye was desorbed using the solvent methanol. The reusability studies of CAB immobilized with dual adsorbent for the adsorption of CR was carried out in three runs.

Keywords: Congo red dye; Calcium alginate entrapped dual adsorbent beads; *Neurospora crassa* dead fungal biomass; Wheat bran; Equilibrium; Kinetics; Isotherms; Thermodynamics

1. Introduction

The worldwide high level of production and use of dyes generates a large amount of colored wastewater [1]. Nowadays, the disposal of dyes and pigments wastewater discharged from industries has received great attention. Synthetic dyes are widely used in different industries such as paper, printing, rubber, food processing, cosmetic, leather, plastics, textile, pharmaceutical, etc. [2]. Currently, more than 1×10^5 dyes are commercially available having various applications with a global annual production in excess of 7×10^5 million tons [3]. Worldwide, 280,000 tons of textile dyes are discharged in industrial effluents every year [4].

* Corresponding author.

Generally, color is visible in the effluents from textile-dyeing processes when the dye concentration is greater than 1 mg L^{-1} and at an average concentration of 300 mg L^{-1} [5]. The effluents of these industries contain highly colored substances and the release of these wastes into receiving water bodies causes severe damages to the environment. Industrial effluents containing synthetic dyes are the major cause of pollution leading to affect the photosynthetic activities of aquatic flora and thereby severely affecting aquatic organisms due to reduced light penetration [6,7]. It is estimated that about 10% of dyes are discharged into the aquatic environment, which is relatively harmful to the human health and aquatic ecosystem due to their high toxicity and carcinogenicity [8]. Most of the azo dyes were reported to be the main cause for bladder cancer in humans, splenic sacromas, hepatocarcinomas, and chromosomal aberration in mammalian cells [9].

Congo red (CR) [1-naphthalene sulfonic acid, 3,3-(4,4-biphenylenebis(azo))bis(4-amino-)disodium salt] is a water soluble diazo anionic dye, synthesized by coupling tetrazotized benzidine with two molecules of naphthionic acid [3]. It has a strong affinity to cellulose fibers and thus is employed in textile industries. It is considered as toxic due to its metabolism to benzidine, a human carcinogen and its exposure causes an allergic reaction. Even a low concentration of CR dye causes the health hazardous symptoms such as difficulties in breathing, diarrhea, vomiting, nausea, and abdominal pain [10]. Therefore, their removal from effluents is of utmost importance before discharge of the wastewater into the environment.

At present, a number of techniques have been employed for the removal of dye contaminants from effluents, which include coagulation, membrane separation, adsorption, advanced oxidation process (photochemical oxidation, ozonation, electrochemical oxidation, Fenton process, irradiation, and sonication), microbial degradation, and biosorption processes [11,12]. Among all these methods, excluding adsorption have some economic and/or environmental drawbacks, such as high capital and operating cost and complexity of the treatment processes. Adsorption is a widely used technique for the removal of dyes in wastewater treatment as it is economical and an environmentally friendly application [7,11]. It eliminates the need for huge sludge-handling processes without discharging any harmful by-products. Well-designed adsorption process has higher efficiency and adsorption capacity resulting in a high-quality effluent after treatment. Furthermore, the adsorbent regeneration is feasible which in turn helps to reduce the adsorbent material cost [13]. Adsorption on commercial activated carbon has been found to be a more efficient process because of its excellent adsorption ability, but it is highly expensive and regeneration of used activated carbon is relatively difficult [14]. To reduce the cost of adsorption treatment process, attention has been focused on the use of inexpensive, abundantly available and more effective adsorbents [11]. These include agricultural by-products, such as barley husks [15], hazelnut shells [16], papaya seeds [17], wheat bran [18], jack fruit peels [19], and peanut hulls [20]. The process cost for the dye removal by adsorption depends mainly on the cost of the adsorbent and its regeneration. In biological treatments, the live biomass is used to biodegrade dye molecules because they can produce enzymes, whereas the dead biomass is used to adsorb the pollutant, which involves physicochemical interactions such as adsorption, deposition, and ion-exchange [12]. Various types of dead fungal biomass such as *Aspergillus fumigatus* [21], *Penicillium simplicissimum* [22], *Rhizomucor pusillius* [23], *Neurospora crassa* [24], *Thamnidium elegans* [25], and *Thuja orientalis* [26], among others, can be used to remove ionic species of adsorbate from dye wastewater.

Most of these batch adsorption studies focused on the use of adsorbent material in powdered form. The use of adsorbent for successful removal of toxic dye in large-scale process application is not practicable because of its smaller particle size, low mechanical strength, low density, and poor rigidity. The separation of adsorbent after adsorption becomes difficult and hence results in loss of adsorbent after regeneration. These problems may be rectified by immobilizing the adsorbent using supporting material such as polymeric matrix [27,28]. Various techniques are used for cell or biomass immobilization, such as flocculation, adsorption on surfaces, covalent bonding to carriers, cross-linking of cells, encapsulation in a polymer gel, and entrapment in a polymeric matrix. Among the various immobilization methods, physical entrapment of adsorbent inside a polymeric matrix is one of the most widely used techniques for immobilization because polymeric matrices can be made as beads to improve its mechanical strength, resistance to the different chemical compounds in the aqueous solutions, minimal clogging under continuous-flow conditions, easier liquid–solid separation, ease of regeneration, and reuse [5,29]. Sodium alginate gel is the most commonly used entrapment matrix. It is a linear binary copolymer carrying carboxyl groups consisting of homopolymeric blocks of (1-4)-linked β-d-mannuronic acid and α-l-guluronic acid [30]. It is a natural polysaccharide extracted from brown seaweed and after processing is available as water-soluble sodium salts. The gelling properties of sodium alginate are mainly affected by the exchange of monovalent sodium ions from the guluronic acid groups with divalent calcium ions and give a gelatinous substance, calcium alginate. As a result of cross-linking, a polymeric network of polysaccharide molecules is formed [29]. Alginate has some unique properties such as, its biocompatibility, hydrophilicity and it is considered to be non-toxic substance [31]. Calcium alginate has been widely used to immobilize activated carbon [32], magnetite nanoparticles [33], and titania nanoparticles [34] to produce different adsorbent materials to remove dyes, heavy metals, and pigments from aqueous solutions. The potential of using dead biomass with wheat bran as effective dual adsorbent to remove azo dyes has not been explored. The dual adsorbent had better adsorption efficiency in the removal of color from dye wastewater when compared with the individual adsorbents and the process with dual adsorbent is rapid [35,36].

The literature survey indicated that adsorption studies of pollutant removal from effluents using dual adsorbent are limited. Biosorption of selected toxic compounds with few types of dead fungal biomass and the use of agricultural by-product as a low-cost adsorbent of dye molecules have been investigated. Therefore, the present study was focused on the removal of CR dye from its aqueous solutions using calcium alginate beads (CAB) immobilized with dual adsorbents that comprises dead fungal biomass of *N. crassa* and wheat bran. *N. crassa* is a filamentous ascomycete

non-pathogenic fungus. Wheat bran is the outer shell of wheat grain, and a by-product of the wheat milling operation; furthermore, it is the economically viable and a most readily available natural material in India.

2. Materials and methods

2.1. Preparation of wheat bran and N. crassa dead biomass dual adsorbent

Wheat bran was obtained from a wheat grinding mill and the filamentous fungus *N. crassa* (MTCC 1852) was procured from Institute of Microbial Technology, Chandigarh, India. The dual adsorbent is the mixture of dead fungal biomass and wheat bran. The optimum amounts of dead biomass and wheat bran were mixed in the proportion of 3:10 (based on weight), which means that 15 g of dead biomass was mixed with 50 g of wheat bran to prepare dead biomass–wheat bran dual adsorbent (DB–WB). The optimum concentration of dead biomass (3 g L^{-1}) and wheat bran (10 g L^{-1}) was added to the dye solution; this gives the maximum percentage of CR decolorization in previous batch studies. The optimum amounts of each adsorbent were obtained from factorial experimental design (central composite design, CCD). The detailed procedure for preparation and evaluation of optimized values of individual adsorbents was given elsewhere [35].

2.2. Preparation of calcium alginate beads immobilized with DB–WB dual adsorbent

The immobilized dual adsorbent CAB was prepared by polymerization route. In a typical procedure, 2% (w/v) slurry of sodium alginate was prepared in hot distilled water at 333 K for 1 h resulting in a transparent and viscous solution [30,37]. After cooling, 4% (w/v) of dual adsorbent powder were added and stirred for 30 min. For polymerization and preparation of beads, the alginate-dual adsorbent slurry was extruded drop by drop into a cold, sterile 0.05 M $CaCl_2$ solution with the help of sterile 12 mL syringe (2 mm, ID) [28,29]. The water-soluble sodium alginate was converted into water-insoluble calcium alginate-entrapped dual adsorbent beads on treatment with calcium chloride [37]. The beads were hardened by re-suspending it into a fresh cold calcium chloride solution for 24 h with gentle agitation [38]. The entrapped CAB beads were washed with distilled water several times to remove unbound calcium chloride from bead surface and kept in an oven at 323 K for 24 h [37].

2.3. Characterization of CAB immobilized with dead biomass–wheat bran dual adsorbent

The prepared CAB immobilized with dual adsorbent was characterized by pore volume, attenuated transmission reflector (ATR), and scanning electron microscopy (SEM) analysis.

2.4. Chemicals required

An anionic dye CR (dye content ≥35%, molecular formula = $C_{32}H_{22}N_6Na_2O_6S_2$, molecular weight = 696.66, λ_{max} = 498 nm) was obtained from Sigma-Aldrich, India. All other chemicals such as sodium alginate, calcium chloride, methanol, ethanol, isopropyl alcohol, butanol, acetone, sodium hydroxide, and hydrochloric acid used were of analytical grade.

2.5. Preparation of CR dye stock solution

A stock solution of 1,000 mg L^{-1} was prepared by dissolving required amount of CR dye powder in distilled water. This stock solution was further diluted with pH adjusted distilled water by adding 0.1 N HCl or 0.1 N NaOH to obtain the required concentration range. After dilution (adjusting the pH), the required pH of the dye solution was measured. The structure of the CR dye is shown in Fig. 1.

2.6. Analytical measurements

The pH of the dye solution was observed by a digital pH meter (Systronics 335). The surface area and pore volume of the CAB immobilized with dual adsorbent were evaluated using a Brunauer–Emmett–Teller (BET) surface analyzer (Smart Instruments, India). A double-beam UV/visible spectrophotometer (Shimadzu UV-1800) was used to determine the unknown residual concentration of CR dye solution. ATR spectra in the transmission range of 400–4,000 cm^{-1} was used to determine the functional groups in the CAB immobilized with dual adsorbent and CR dye loaded CAB immobilized with dual adsorbent using ATR spectroscopy (IR Prestige-21, Shimadzu, Japan). The surface morphology of CAB (blank) and CAB immobilized with DB–WB dual adsorbent were analyzed by field emission scanning electron microscopy/energy dispersive X-ray spectroscopy (FESEM/EDS; Carl Zeiss – FESEM attached with Oxford Instruments EDS, Germany).

2.7. Adsorption experiments

Batch experiments were performed to investigate the percentage adsorption of CR as a function of initial pH, initial dye concentration, entrapped dual adsorbent loading in CAB, adsorbent dosage, and temperature. Adsorption equilibrium experiments were conducted by stirring CR dye aqueous solutions at 180 rpm for 24 h at 303 K with initial dye concentration of 50–400 mg L^{-1} in each flask containing fixed quantity of CAB immobilized with dual adsorbent dosage. The adsorption kinetics experiments were performed at various dye concentrations from 50 to 400 mg L^{-1} with a fixed dual adsorbent dosage and at constant temperature. A known amount of solution was withdrawn at regular time intervals. The amount of CR dye adsorbed onto a unit mass of entrapped dual adsorbent at equilibrium and the percentage adsorption [6,39] were determined using Eqs. (1) and (2), respectively.

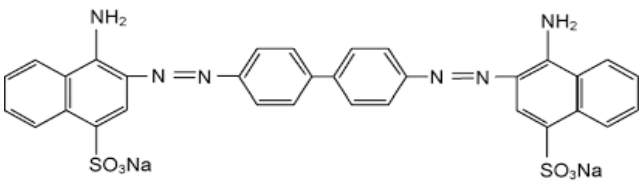

Fig. 1. Molecular structure of Congo red dye.

$$q_e = \frac{(C_o - C_e)V}{W} \quad (1)$$

$$\%\ \text{CR dye adsorption} = \frac{(C_o - C_e)\times 100}{C_o} \quad (2)$$

where C_o and C_e are the initial and equilibrium dye concentrations in solution (mg L^{-1}), V is the volume of dye solution (L), and W is the mass of dry CAB immobilized with DB–WB dual adsorbent (g).

2.8. Experimental design and optimization of process parameters

Response surface methodology was employed to optimize process parameters within the limited number of runs and investigate the relationship between percentage adsorption and operating variables. The experimental design was constructed through Minitab 16 statistical software and CCD was applied to conduct adsorption experiments. The CCD utilizes multilevel design with axial points along with center point to fit the quadratic model [40]. The influencing factors such as initial pH (X_1), initial dye concentration (X_2), entrapped dual adsorbent dosage (X_3), and agitation speed (X_4) were chosen as the independent variables while the percentage adsorption was set as the response (dependent) variable. The numbers of experimental runs are calculated by the following Eq. (3) [41]:

$$N = 2^f + 2f + N_o \quad (3)$$

where f represents the number of variables, 2^f represents the number of factorial points, $2f$ represents the axial points, and the center points are represented by N_o. A total of 31 experiments were conducted including 16 factorial points, 8 axial points, and 7 center points using 2^4 full factorial design. The repetition of central point gives an estimated error. The levels of independent variables were coded as –2 (very low), –1 (low), 0 (central point), 1 (high), and 2 (very high). The coded values of process variables were obtained from the following Eq. (4) [42]:

$$x_i = \frac{(X_i - X_o)}{\delta X} \quad (4)$$

where x_i is the dimensionless value of a process variable; X_i is the real value of an independent variable; X_o is the value of X_i at the center point; and δX denotes the step change. The polynomial expression for the relation between the independent and response variables is given as [42]:

$$Y = \beta_o + \sum \beta_i x_i + \sum \beta_{ii} x_i^2 + \sum \beta_{ij} x_i \quad (5)$$

where Y is the predicted response variable of percentage adsorption; β_o is the offset term; and β_i, β_{ii}, and β_{ij} are the regression coefficients for linear, quadratic, and interaction effects, respectively. Analysis of variance (ANOVA) is a statistical technique that is widely employed to assess the significance and validation of model in the adsorption process.

2.9. Desorption studies and reusability of the CAB immobilized with DB–WB dual adsorbent

Desorption of CR from CAB immobilized with dual adsorbent was investigated using various desorbing agents, such as methanol, ethanol, isopropyl alcohol, butanol, acetone, and 1 M NaOH [43–45]. In a typical desorption experiment, the above mentioned desorbing agents were added to the entrapped dual adsorbent loaded with adsorbed dye and agitated for a sufficient duration in separate batches. The detailed desorption experiment procedure has been reported elsewhere [35]. The efficiency of desorbed dye from the entrapped dual adsorbent was calculated using the following Eq. (6) [7]:

$$\text{Desorption efficiency} = \frac{\text{Amount of CR dye desorbed}}{\text{Amount of CR dye adsorbed}} \times 100 \quad (6)$$

2.10. Error analysis

To identify the suitable isotherm for adsorption of CR onto CAB immobilized with dual adsorbent, the chi-square (χ^2) test was carried out using the experimental data, to find the best adsorption isotherm model. The chi-square test statistic (χ^2) is basically the sum of squares of the difference between the experimental data and data obtained by calculating from models, with each squared difference divided by the corresponding data obtained by calculating from models. If data from the model are similar to the experimental data, χ^2 will be a small number; if they are different, χ^2 will be a large number. The chi-square (χ^2) value was calculated using the following Eq. (7) to evaluate the best fit isotherm model [7].

$$\chi^2 = \sum \left[\frac{\left(q_{e,\text{exp}} - q_{e,\text{cal}}\right)^2}{q_{e,\text{cal}}} \right] \quad (7)$$

where $q_{e,\text{exp}}$ and $q_{e,\text{cal}}$ are the experimental adsorption capacities of CR (mg g^{-1}) at equilibrium and the corresponding values that are obtained from the kinetic models.

3. Results and discussion

3.1. Characterization of the CAB immobilized with DB–WB dual adsorbent

The average diameter of immobilized dual adsorbent bead was found to be 2.4 mm. The physical characteristics of the blank CAB and CAB immobilized with dual adsorbent are reported in Table 1. The BET surface area and pore volume of the entrapped dual adsorbent beads at 303 K were 0.5 $m^2\ g^{-1}$ and 0.8 $mm^3\ g^{-1}$, respectively. ATR spectra of the CAB immobilized with dual adsorbent before and after CR dye adsorption are shown in Figs. 2(a) and (b), respectively. The ATR spectrum of the entrapped dual adsorbent before adsorption shows a broad and strong peak at 3,333 cm^{-1}, representing the O–H stretching vibration of bonded hydroxyl groups. The short peak observed at 2,953 cm^{-1} was due to the C–H symmetric stretching of methyl groups. The strong band at 1,597 cm^{-1} was characteristic of stretching vibration of C=O group from carboxylic acid with intermolecular hydrogen

Table 1
Physical properties of calcium alginate blank beads and CAB immobilized with DB–WB dual adsorbent

Parameters	Blank beads	DB–WB dual adsorbent loading in CAB at 303 K		4% (w/v) dual adsorbent loading in CAB at 333 K
		4% (w/v)	10% (w/v)	
BET surface area (m^2 g^{-1})	1.66	0.5	0.23	1.05
Pore volume (mm^3 g^{-1})	2.80	0.8	0.3	1.20

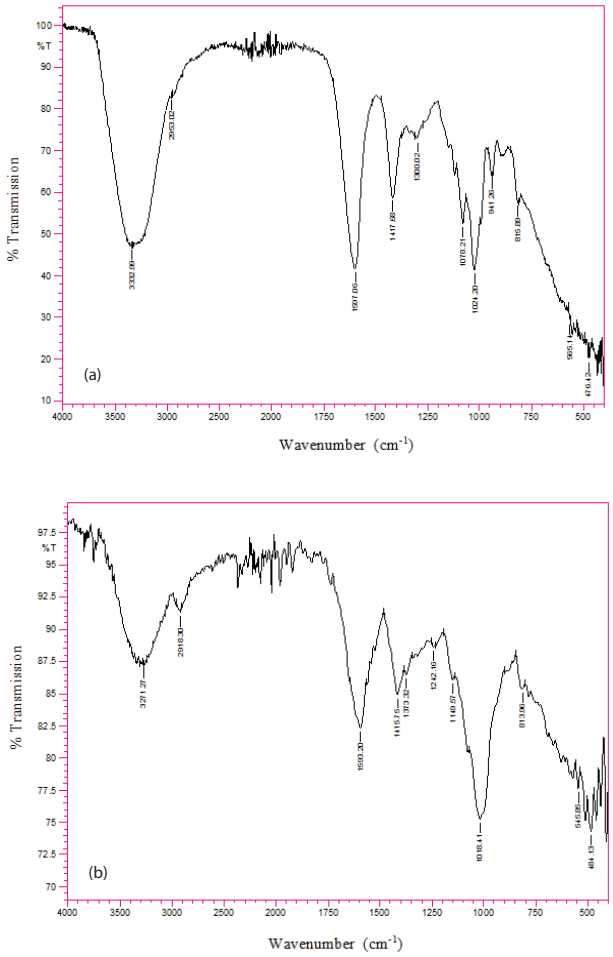

Fig. 2. (a) ATR spectrum of CAB immobilized with dual adsorbent before CR dye adsorption. (b) ATR spectrum of CAB immobilized with dual adsorbent after CR dye adsorption.

bond. The asymmetric deformation of $–CH_2$ group was observed by the peak at 1,418 cm^{-1}. The stretching vibration of carboxylate ion was detected by the peak at 1,300 cm^{-1}. The wavenumber observed at 1,078 cm^{-1} was assigned to the C–O stretching vibration of carboxylic acid and alcoholic groups. The bending vibrations of –OH and stretching vibrations of C–O–C were observed in the form of the peak at 1,024 cm^{-1}. The absorption band at the frequency zone of 800–700 cm^{-1} is assigned to the stretching vibration of C–Cl aliphatic chloro compounds. A short peak at 565 cm^{-1} corresponds to =C–H bending vibrations of alkynes. The interaction between the carboxylic groups of alginate and the surface hydroxyl groups of DB–WB dual adsorbent may be the expected reason for attachment of alginate with dual adsorbent. After adsorption, the significant changes have been observed in band intensities of hydroxyl (3,271 cm^{-1}), methyl (2,918 cm^{-1}), carboxylic acid (1,593 cm^{-1}), and alcoholic (1,149 cm^{-1}) groups in the ATR spectra of CR-loaded CAB immobilized with dual adsorbent (Fig. 2(b)). The analysis of the ATR spectral results in terms of frequency shifts indicate that these functional groups above mentioned are responsible for CR dye uptake. A frequency shift was observed for all band positions after CR dye adsorption [3,7,39,46].

The surface morphology of dry beads was observed using SEM. The SEM images of the CAB (blank beads) and CAB immobilized with dual adsorbent are shown in Figs. 3(a) and (b), respectively. The calcium alginate blank beads and entrapped dual adsorbent beads were nearly spherical in shape (Figs. 3(a) and (b)). The CAB has relatively smooth surfaces as seen in Fig. 3(a). The presence of rough fibrous morphology on the surface of the entrapped dual adsorbent after immobilization was evident from Fig. 3(b). Rough surfaces are favorable for molecular diffusion and good possibility for CR dye to be adsorbed into these entrapped dual adsorbent.

3.2. Analysis of batch adsorption studies

Batch experiments were conducted by varying the level of one factor and keeping the level of other factors constant on the other hand. The experiments were conducted by varying operational factors such as pH, initial dye concentration, entrapped dual adsorbent dosage and agitation speed on CR dye adsorption process.

3.2.1. Effect of initial pH

The initial pH of the aqueous solution is an important parameter in the adsorption process because it can affect the interaction of the surface functional groups of the adsorbent and the adsorbate. To analyze the effect of the initial pH on dye adsorption under a strongly acidic pH was difficult because of the formation of protonated species, which may lead to a change in the structure of the dye. The CR dye in aqueous solution was black in color at acidic pH (<5), due to the formation of a quinonoid structure [47]. The red color remained stable in the pH range of 6–12. Therefore, the effect of initial solution pH on the adsorption of CR on CAB immobilized with dual adsorbent from aqueous solution was investigated in the pH range between 6 and 12. As shown in Fig. 4, the percentage adsorption of CR decreased from 75.69% to 26.85% when the solution pH increased from 6 to 12. The maximum adsorption of CR was observed at pH 6. Hence, all the succeeding investigations were performed at pH 6. At pH 6, a significant electrostatic attraction exists

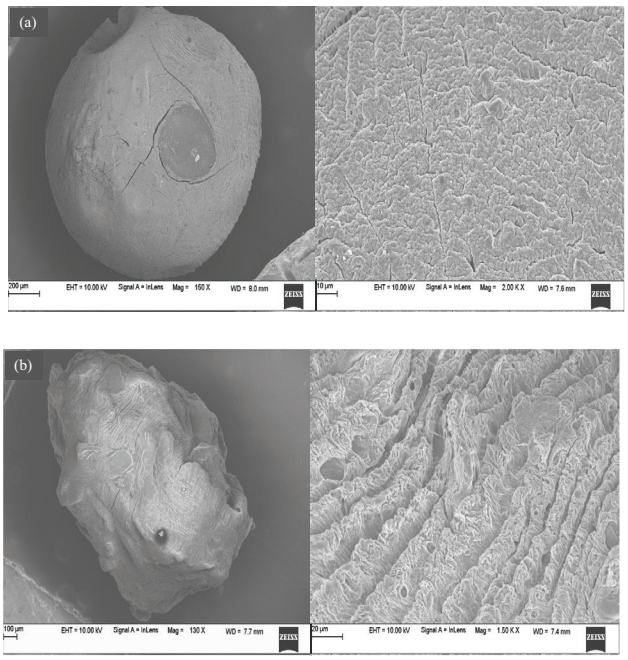

Fig. 3. (a) SEM micrograph of calcium alginate blank beads (before entrapment of dual adsorbent). (b) SEM micrograph of CAB immobilized with dual adsorbent before CR dye adsorption.

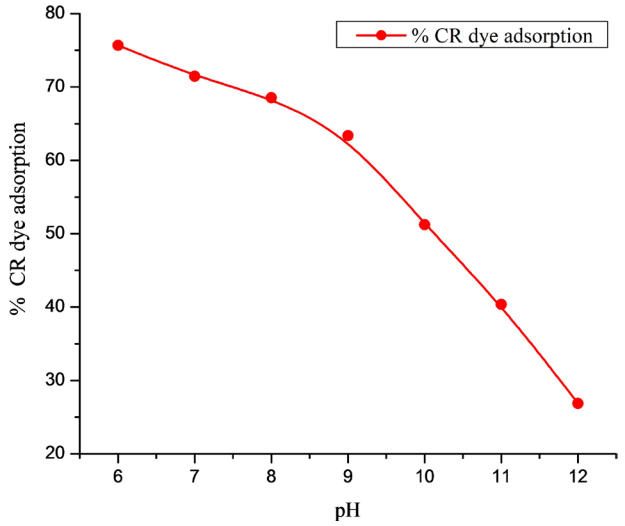

Fig. 4. Effect of initial pH on CR dye adsorption by dual adsorbent entrapped in CAB (initial dye concentration: 300 mg L^{-1}; dual adsorbent loading in CAB: 2% (w/v); entrapped dual adsorbent dosage: 5 g L^{-1}; agitation speed: 180 rpm; temperature: 303 K; and contact time 10 h).

between the positively charged surfaces of CAB immobilized with dual adsorbent and anionic CR dye molecules. As the pH of the solution increases, the number of negatively charged sites increases and the number of positively charged sites decrease. A negatively charged surface sites on the entrapped dual adsorbent does not favor the adsorption of the CR dye anions due to the electrostatic repulsion. Also, lower percentage adsorption of CR observed at basic pH may be due to competition between the excess hydroxyl ions and the negatively charged dye ions for the adsorption active sites. Therefore, the possible mechanisms of CR dye adsorption may be electrostatic interactions between protonated adsorption sites of the adsorbent and negatively charged dye anions in addition to hydrogen bonding forces [3,7].

3.2.2. Effect of dead biomass–wheat bran dual adsorbent loading in CAB

To optimize the dual adsorbent loading in CAB polymeric matrix, entrapped dual adsorbents were prepared with varying compositions of dual adsorbent in CAB. The effect of dual adsorbent loading in CAB on adsorption of CR was studied from 1% to 10% (w/v). Fig. S1 of supplementary materials shows that an increase in dual adsorbent loading yields better adsorption. However, loading above an optimal limit decreases the percentage dye adsorption, which may be attributed to the difference in porosity of the beads when a higher quantity of dual adsorbent was loaded. The optimum dual adsorbent loading was found to be 4% (w/v). As the dual adsorbent dose was increased from 4% to 10% (w/v) in CAB, the pore volume and surface area of the bead decreased from 0.8 to 0.3 mm^3 g^{-1} and 0.5 to 0.23 m^2 g^{-1}, respectively (Table 1). It may affect the free transport of dye anions to the interior binding sites through the formation of a physical boundary layer and agglomeration of dual adsorbent particles in CAB. The increase in dose of adsorbent, in relation to the amount of polymer, reduced the surface area of the bead [48]. A similar observation has been reported elsewhere [28].

3.2.3. Effect of entrapped dual adsorbent dosage

The effect of entrapped dual adsorbent dosage is also an important parameter as it determines the percentage adsorption and adsorption capacity of an adsorbent for a given initial dye concentration. The influence of entrapped dual adsorbent on CR adsorption was analyzed by varying the adsorbent amount from 0.1 to 1.0 g per 100 mL of dye solution with an initial dye concentration of 300 mg L^{-1} at pH 6. From Fig. S2 of supplementary materials, it can be seen that the removal efficiency of CR increased from 67.63% to 87.42% with the increase in the entrapped dual adsorbent dosage. This is because, increased adsorbent surface and availability of more adsorption active sites at higher concentrations of the adsorbent for the removal of CR dye. However, if the adsorption capacity was expressed as amount of dye adsorbed per gram of the material (q_e), the capacity decreased from 202.89 to 26.22 mg g^{-1} with the increase in the entrapped dual adsorbent dosage (Fig. S2 of supplementary materials). This is mainly due to the split in the flux or concentration gradient between the adsorbate concentration in the solution and that at the surface of the dual adsorbent. Thus, the competition for the availability of active sites for the adsorption of dye decreases with the increase in the adsorbent dosage (increase of unsaturation of adsorption binding sites through the adsorption reaction). In other words, this may be due to the particle interactions, such as aggregation or overlapping of adsorption sites, resulting from high adsorbent concentration. Such aggregation would lead to decrease in total active surface area of the adsorbent and an increase in diffusion path length [49,50]. Hence, the amount of CR dye adsorbed

onto a unit weight of entrapped dual adsorbent (q_e) gets decreased with increase in adsorbent dosage.

3.2.4. Effect of agitation speed

The influence of agitation speed in a batch adsorption process is important to overcome the external mass transfer resistance. Effect of agitation speed on CR dye adsorption was evaluated by varying the agitation speed from 0 to 250 rpm at 303 K. The increase in the agitation speed increased the percentage adsorption of CR dye from 34.22% to 85.98% (Fig. S3 of supplementary materials). The maximum percentage adsorption occurred at 250 rpm. Under static condition (0 rpm), the percentage adsorption was 34.22%. The increase in removal efficiency may be due to increase in turbulence attributable to decrease in the film boundary layer thickness (film resistance) surrounding the CAB entrapped with dual adsorbent particles, thus increasing external film diffusion and uptake of CR dye molecules. This phenomenon may be explained by increasing the contact surface of solid–liquid and favoring the transfer of dye molecules to the entrapped dual adsorbent binding sites [51,52].

3.3. Analysis of factorial experimental design and optimization of process parameters

Various groups of independent variables were used to study the mutual effect of different parameters using statistically designed experiments. The experimental ranges and levels of various independent variables in CR dye adsorption are given in Table 2. The experimental and predicted values of percentage adsorption of CR are given in Table 3. The results were analyzed by ANOVA and are given in Table 4. These analyses were done by means of Fisher's *F*-test and Student's *T*-test. The probability level, *P*, was used to verify the significance of each of the interactions among the factors and *T* tests were applied to evaluate the significance of the regression coefficients of the parameters. Larger magnitude of *T* and lower values of *P* ($P < 0.05$) indicates that the linear, quadratic, and interaction effects are more significant in the chosen model at the corresponding coefficient terms. The suitability of the response surface model was assessed by the values of regression coefficient (R^2), coefficient of variation, adequate precision and by the analysis of lack of faith.

The coefficients for the linear effect of initial dye concentration (X_2), entrapped dual adsorbent dosage (X_3), and agitation speed (X_4) were the first important factors ($P = 0.000$). Initial pH of aqueous solution (X_1) was the second important factor ($P = 0.001$). The coefficients for the linear effect of all the factors signified the effect of adsorption of CR dye on entrapped dual adsorbent. The coefficients of the quadratic effect of initial dye concentration (X_2), and entrapped dual adsorbent dosage (X_3) were the first important factors ($P = 0.000$), while agitation speed (X_4) and pH (X_1) were the second and third important factors ($P = 0.001$, $P = 0.011$), respectively. The coefficient of the interaction effect between pH (X_1) and entrapped dual adsorbent dosage (X_3) was found to be significant ($P = 0.002$). However, the coefficients of the other interactive effects (X_1X_2, X_1X_4, X_2X_3, X_2X_4, and X_3X_4) among the variables did not appear to be significant. The larger value of $F_{\text{statistics}}$ indicates that most of the variation in the response can be explained by the regression model equation. The regression model (Eq. (8)) for percentage CR dye adsorption is as follows:

$$\begin{aligned}\%\ \text{CR adsorption} = {} & 82.5371 - 1.7254X_1 - 5.0938X_2 \\ & + 5.9038X_3 + 2.6146X_4 - 1.1019X_1^2 \\ & - 2.7694X_2^2 - 3.3994X_3^2 - 1.4569X_4^2 \\ & - 0.3831X_1X_2 - 1.9144X_1X_3 - 0.1631X_1X_4 \\ & - 0.5369X_2X_3 + 0.2494X_2X_4 + 0.9231X_3X_4\end{aligned} \quad (8)$$

The regression coefficient, R^2 quantitatively evaluates the correlation between the experimental data and the predicted responses. The predicted values match the experimental values reasonably well with R^2 of 0.9720, which indicates that 97.20% of the variations in response could be described by this model and this also means that the model does not explain only about 2.8% of the variation. Adjusted R^2 (0.9475) is a tool to measure the goodness of fit, but it is more suitable for comparing models with various operating parameters. It corrects the R^2 value for the number of terms in the model and the sample size by using the degrees of freedom in its computations. Predicted R^2 (0.8386) can prevent overfitting the model and can be calculated from predicted residual error sum of squares (PRESS) statistics. Larger values of predicted R^2 suggest models of greater predictive ability. This may indicate that an overfitted model will not predict any new observations nearly as well as it fits the existing data. The adequacy of the model was evaluated by the residuals which is the difference between observed and the predicted response values. The ANOVA table shows the residual error, which measures the elements of variation in the response that cannot be explained by the model, and their occurrence in a normal distribution.

Fig. 5(a) shows that the observed residuals are plotted against the expected values, given by normal distribution. It is a useful way to examine the hypothesis of normality of

Table 2
Experimental range and levels of independent variables for CR dye adsorption by CAB immobilized with dual adsorbent

Independent variables	Range and level				
	–2	–1	0	1	2
Initial pH (X_1)	5.6	5.8	6.0	6.2	6.4
Initial dye concentration, mg L^{-1} (X_2)	200	250	300	350	400
Entrapped dual adsorbent dosage, g (X_3)	0.1	0.3	0.5	0.7	0.9
Agitation speed, rpm (X_4)	120	150	180	210	240

Table 3
Four-factor full factorial central composite design matrix and responses for CR dye adsorption by CAB immobilized with dual adsorbent

Run no.	X_1	X_2 (mg L^{-1})	X_3 (g)	X_4 (rpm)	% CR dye adsorption	
					Experiment	Predicted
1	1	–1	–1	1	73.54	74.31
2	1	–1	–1	–1	71.15	71.76
3	–1	1	1	1	81.19	82.06
4	0	0	0	0	82.58	82.54
5	–1	1	1	–1	72.96	74.16
6	1	–1	1	–1	77.90	78.96
7	–2	0	0	0	84.46	81.58
8	1	1	1	–1	66.62	66.44
9	0	0	0	0	82.52	82.54
10	1	–1	1	1	83.62	85.21
11	–1	–1	1	1	89.32	92.05
12	–1	–1	–1	1	71.84	73.50
13	0	0	0	0	82.46	82.54
14	0	2	0	0	61.24	61.27
15	1	1	–1	–1	62.14	61.38
16	0	0	2	0	84.16	80.75
17	0	0	0	0	82.52	82.54
18	–1	–1	1	–1	83.65	85.15
19	0	0	–2	0	57.16	57.13
20	0	0	0	0	82.49	82.54
21	0	0	0	2	85.22	81.94
22	0	0	0	–2	71.64	71.48
23	1	1	1	1	72.18	73.68
24	0	0	0	0	82.63	82.54
25	0	0	0	0	82.56	82.54
26	–1	1	–1	1	64.74	65.65
27	2	0	0	0	75.24	74.68
28	0	–2	0	0	85.12	81.65
29	1	1	–1	1	64.96	64.93
30	–1	–1	–1	–1	69.82	70.29
31	–1	1	–1	–1	61.56	61.44

the observations. The residuals in the plot follow a straight line and are normally distributed. It can be observed that the residuals from the analysis do not have any effect on the result and are the best residuals. Fig. 5(b) depicts the plot of residuals based on the predicted amounts of percentage adsorption. The residuals in this plot appear to be randomly scattered above and below the zero line. The greater spread of residuals in this plot signifies the increase in the fitted values. Fig. 5(c) shows the histogram of the residuals. A long tail in the plot indicates the skewed distribution. The one or two bars that are far from the others may be outliers. The non-uniform bars in the plot represent the more fitted values. Fig. 5(d) illustrates the residuals in the order of the corresponding observations. It was observed that the residuals in the plot fluctuate in a random pattern around the zero line in the order of observation, and this was used to determine the non-random error [53].

3.3.1. Contour and response surface plots

The contour plots of mutual interactions between the variables for percentage adsorption of CR were found to be elliptical, as shown in Figs. 6(a)–(d). The coordinates of the central point in each of these plots indicate the optimal value of the respective constituents. The stationary point or central point is the point at which the slope of the contour is zero in all directions. The maximum predicted percentage adsorption is shown by the minimum curvature of the contour plot. Fig. 6(a) shows that the highest percentage adsorption using CAB immobilized with dual adsorbent occurs when the dye concentration ranges between 225 and 275 mg L^{-1} and the pH ranges from 5.75 to 5.95. Fig. 6(b) shows that the maximum predicted response occurs when the entrapped dual adsorbent dosage ranges between 0.45 and 0.9 g and the pH in the range of 5.6–6.2. Fig. 6(c) shows that the maximum predicted yield occurs when the entrapped dual adsorbent

Table 4
ANOVA for percentage adsorption of CR dye using CAB immobilized with DB–WB dual adsorbent from the data of CCD experiments

Term	Coefficient	SE of coefficient	$T_{statistics}$	DF	Seq SS	Adj SS	Adj MS	$F_{statistics}$	Probability
Constant	82.5371	0.7695	107.257						
Regression				14	2,300.80	2,300.80	164.343	39.65	0.000
X_1	–1.7254	0.4156	–4.152	1	71.45	71.45	71.450	17.24	0.001
X_2 (mg L^{-1})	–5.0938	0.4156	–12.257	1	622.71	622.71	622.711	150.22	0.000
X_3 (g)	5.9038	0.4156	14.206	1	836.50	836.50	836.502	201.80	0.000
X_4 (g)	2.6146	0.4156	6.291	1	164.07	164.07	164.065	39.58	0.000
$X_1 \times X_1$	–1.1019	0.3807	–2.894	1	34.72	34.72	34.720	8.38	0.011
X_2 (mg L^{-1}) × X_2 (mg L^{-1})	–2.7694	0.3807	–7.274	1	219.32	219.32	219.316	52.91	0.000
X_3 (g) × X_3 (g)	–3.3994	0.3807	–8.928	1	330.45	330.45	330.448	79.72	0.000
X_4 (g) × X_4 (g)	–1.4569	0.3807	–3.827	1	60.70	60.70	60.695	14.64	0.001
$X_1 \times X_2$ (mg L^{-1})	–0.3831	0.5090	–0.753	1	2.35	2.35	2.349	0.57	0.463
$X_1 \times X_3$ (g)	–1.9144	0.5090	–3.761	1	58.64	58.64	58.637	14.15	0.002
$X_1 \times X_4$ (g)	–0.1631	0.5090	–0.320	1	0.43	0.43	0.426	0.10	0.753
X_2 (mg L^{-1}) × X_3 (g)	–0.5369	0.5090	–1.055	1	4.61	4.61	4.612	1.11	0.307
X_2 (mg L^{-1}) × X_4 (g)	0.2494	0.5090	0.490	1	1.00	1.00	0.995	0.24	0.631
X_3 (g) × X_4 (g)	0.9231	0.5090	1.814	1	13.63	13.63	13.635	3.29	0.089
Residual error				16	66.32	66.32	4.145		
Lack-of-fit				10	66.30	66.30	6.630	2,015.03	0.000
Pure error				6	0.02	0.02	0.003		
Total				30	2367.12				

Note: Regression coefficient $R^2 = 0.9720$, R^2 (pred) = 0.8386, R^2 (adj) = 0.9475, $S = 2.03599$, PRESS = 381.938.
SE, standard error of coefficient; DF, degrees of freedom; Seq SS, sequential sum of squares; Adj SS, adjusted sum of squares; Adj MS, adjusted mean squares; PRESS, predicted residual sum of squares; *S*, value of *S* chart.

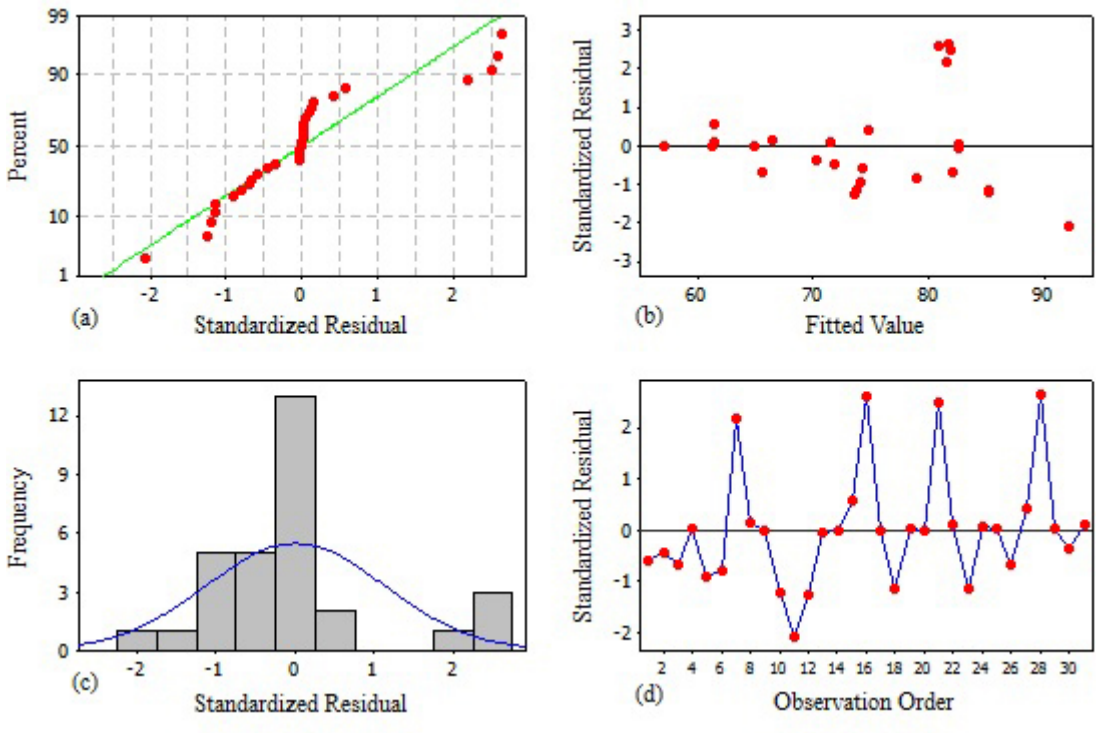

Fig. 5. Residual plots for adsorption of Congo red dye by CAB immobilized with dual adsorbent. (a) Normal probability plot of residuals. (b) Residuals vs. fitted values. (c) Frequency of observation vs. residuals. (d) Residuals vs. the order of the data.

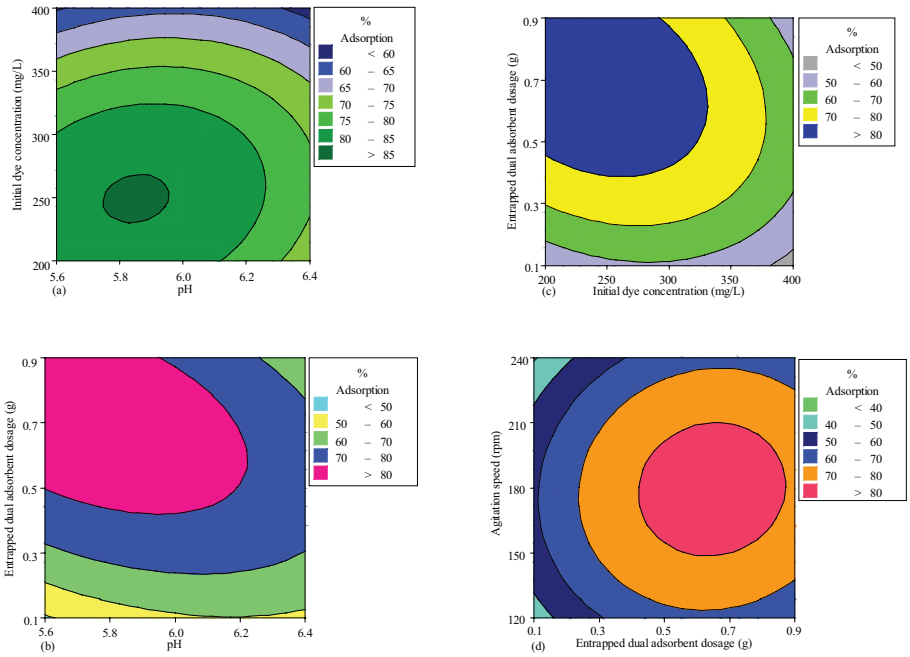

Fig. 6. Contour plots for interactive effect of (a) initial dye concentration and pH, (b) entrapped dual adsorbent dosage and pH, (c) entrapped dual adsorbent dosage and initial dye concentration, and (d) agitation speed and entrapped dual adsorbent dosage.

dosage ranges between 0.45 and 0.9 g and the initial dye concentration in the range of 200–325 mg L^{-1}. Fig. 6(d) shows that the maximum predicted percentage adsorption occurs when the agitation speed ranges between 150 and 200 rpm and the entrapped dual adsorbent dosage ranges from 0.45 to 0.85 g, and the effect is not very significant. A similar observation has been reported elsewhere [35,42].

Fig. 7(a) shows the surface plot of the response variable as a function of pH and initial dye concentration. It clearly shows that the percentage adsorption of CR increased with

the decrease in the pH and initial dye concentration. The pH in the range of 5.75–5.95 does not have significant effect, while a dye concentration ranges between 200 and 400 mg L^{-1} has a significant effect on the maximum adsorption of the CR using CAB immobilized with dual adsorbent. Fig. 7(b) shows that with an increase in the amount of entrapped dual adsorbent and decrease in pH, the adsorption efficiency improves. The response plot of pH in the range of 5.6–6.2 does not have significant effect, while an entrapped dual adsorbent dosage ranges between 0.1 and 0.9 g has a significant effect on the maximum adsorption of the CR dye. Similarly, the surface plot (Fig. 7(c)) of the entrapped dual adsorbent dosage in the range of 0.1–0.9 g vs. the initial dye concentration in the range of 200–400 mg L^{-1}; and agitation speed in the range of 120–240 rpm vs. entrapped dual adsorbent dosage in the range of 0.1–0.9 g (Fig. 7(d)) shows a significant effect on the percentage adsorption of the CR from aqueous solution. The optimal response values obtained from these plots are in close agreement with those values obtained from the experiment and regression model equation. This shows that the model properly explains the influence of the chosen variables on the percentage of CR dye adsorption. The optimal values of the process independent variables for maximal percentage of CR dye removal are given in Table 5. A similar observation has been reported elsewhere [35,40,53].

3.4. Adsorption isotherms

The equilibrium data commonly known as adsorption isotherms are basic requirements for designing the adsorption systems. These data provide information on the capacity of the adsorbent or the amount required to remove the mass of pollutant from aqueous solution under the system conditions. The adsorption isotherm indicates how the adsorption molecules distribute between the liquid phase and the solid phase when the adsorption process reaches an equilibrium state [54]. The experimental adsorption data were analyzed by Freundlich, Langmuir, and Temkin isotherm models. Linear regression is commonly used to determine best fit isotherm model, and the method of least squares has been widely used for obtaining the isotherm constants.

The Freundlich model is based on the assumption that adsorption occurs on a heterogeneous solid surface having unequally available sites with different energies of adsorption over the surface and the possibility of multilayer adsorption. It is assumed that the adsorbent–adsorbate interaction decreases with the decrease in available binding sites. The linear expression of this model equation (Eq. (9)) is given by [55]:

$$\log q_e = \log K_F + \frac{1}{n}\log C_e \tag{9}$$

where K_F and $1/n$ are the Freundlich isotherm constant (L g^{-1}) and heterogeneity factor, respectively, which indicate the capacity and intensity of adsorption. The value of n is an indication of the favorability of adsorption. When $0 < 1/n < 1$,

Table 5
Optimal values of the process independent variables for maximum percentage adsorption of CR dye

Process parameters	Optimum value	% adsorption of CR dye
Initial pH (X_1)	5.8	89.32
Initial dye concentration, mg L^{-1} (X_2)	250	
Entrapped dual adsorbent dosage, g (X_3)	0.7	
Agitation speed, rpm (X_4)	210	

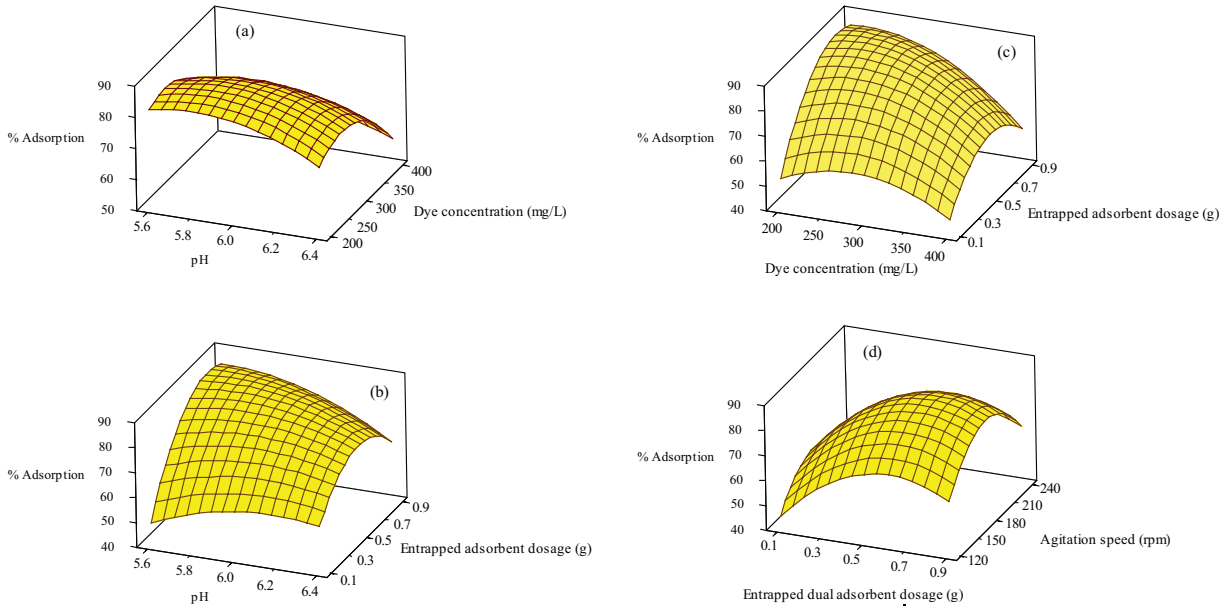

Fig. 7. Surface plots for interactive effect of (a) initial dye concentration and pH, (b) entrapped dual adsorbent dosage and pH, (c) entrapped dual adsorbent dosage and initial dye concentration, and (d) agitation speed and entrapped dual adsorbent dosage.

the adsorption is favorable; $1/n = 1$, the adsorption is homogeneous and there is no interaction among the adsorbed species; $1/n > 1$, the adsorption is unfavorable. The values K_F and $1/n$ can be determined from the intercept and slope of the linear plot of $\log q_e$ vs. $\log C_e$ (Fig. 8). The Langmuir isotherm assumes that the surface of any adsorbent material contains a fixed number of active sites and saturation of these active sites stops the adsorption of the adsorbate. This indicates that the adsorption occurs until a monolayer of adsorption is completed and after completion of adsorption, no more interaction between the adsorbent and adsorbate molecules (adsorption takes place at specific homogeneous sites within the adsorbent and active binding site becomes inactive once the adsorbate molecule is adsorbed onto it). The energy of adsorption is constant and no transmigration of adsorbate occurs on the surface. The linear form of Langmuir isotherm model is expressed as [56]:

$$\frac{1}{q_e} = \frac{1}{q_{\max}} + \frac{1}{q_{\max} K_L C_e} \tag{10}$$

where K_L is the Langmuir isotherm constant (L mg^{-1}) and $q_{\max}$ is the theoretical maximum saturation capacity at equilibrium corresponding to the monolayer coverage on the surface (mg g^{-1}). The linear plot of $1/q_e$ vs. $1/C_e$ permits the determination of $q_{\max}$ and K_L from the intercept and slope of the plot (Fig. 9). The essential characteristics of the Langmuir isotherm can be expressed in terms of a dimensionless separation factor, R_L, also known as the equilibrium parameter which is defined by the following Eq. (11) [57]:

$$R_L = \frac{1}{1 + K_L C_o} \tag{11}$$

The value of R_L indicates the shape of the isotherms to be either irreversible ($R_L = 0$), favorable ($0 < R_L < 1$), linear ($R_L = 1$) or unfavorable ($R_L > 1$). The Temkin isotherm model contains a factor that explicitly takes into the account of adsorbing species–adsorbate interactions. By ignoring the extremely low and large value of concentrations, the model assumes that (i) heat of adsorption of all molecules in the layer would decrease linearly rather than logarithmic with coverage as implied in Eq. (12) and (ii) adsorption is characterized by a uniform distribution of binding energies, up to some maximum binding energy. A linear form of the Temkin isotherm model is represented by the following linear Eq. (12) [58]:

$$q_e = \frac{RT}{b_T} \ln K_T + \frac{RT}{b_T} \ln C_e \tag{12}$$

where K_T is the Temkin isotherm constant (L g^{-1}), $\frac{RT}{b_T}$ indicates the heat of adsorption, b_T is the adsorption energy (kJ mol^{-1}), T is the absolute temperature (K), and R is the universal gas constant (J mol^{-1} K^{-1}). The plot of q_e vs. $\ln C_e$ yields a straight line for which the slope b_T and intercept K_T are estimated (Fig. S4 of supplementary materials).

3.4.1. Inference from adsorption isotherm models

The parameters calculated from regressive analysis of various adsorption isotherm models were reported in Table 6. It shows that the best fitted adsorption isotherms considering the regression coefficient, R^2, and chi-square, χ^2, values obtained for the isotherms were to be in the order of prediction precision: Langmuir > Freundlich > Temkin isotherms. A higher value of the regression coefficient ($R^2 = 0.9987$ and lower value of chi-square ($\chi^2 = 0.9687$) were found in the Langmuir model, compared with the Freundlich ($R^2 = 0.9811$, $\chi^2 = 1.3302$) and Temkin isotherm ($R^2 = 0.9758$, $\chi^2 = 8.9126$) models. It suggests that the equilibrium data for CR adsorption by CAB immobilized with dual adsorbent was fitted with Langmuir isotherm model followed by Freundlich and Temkin models. According to the assumption of Langmuir isotherm, the

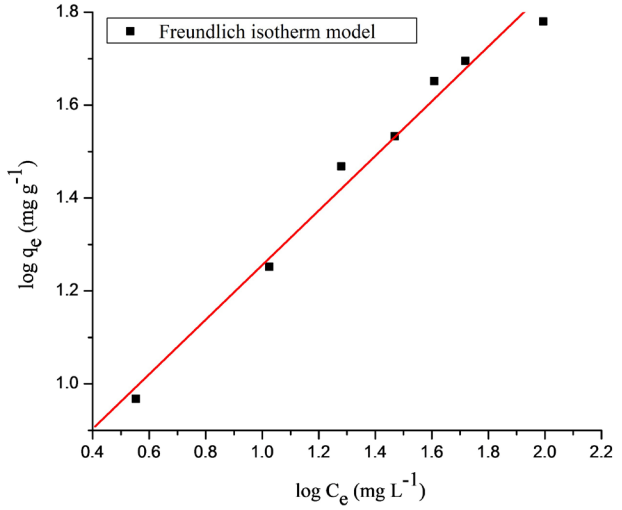

Fig. 8. Freundlich isotherm plot for CR dye adsorption by CAB immobilized with dual adsorbent (initial pH: 6; CR dye concentration: 50–400 mg L^{-1}; dual adsorbent loading in CAB: 4% (w/v); entrapped dual adsorbent dosage: 5 g L^{-1}; agitation speed: 180 rpm; temperature: 303 K; and contact time: 24 h).

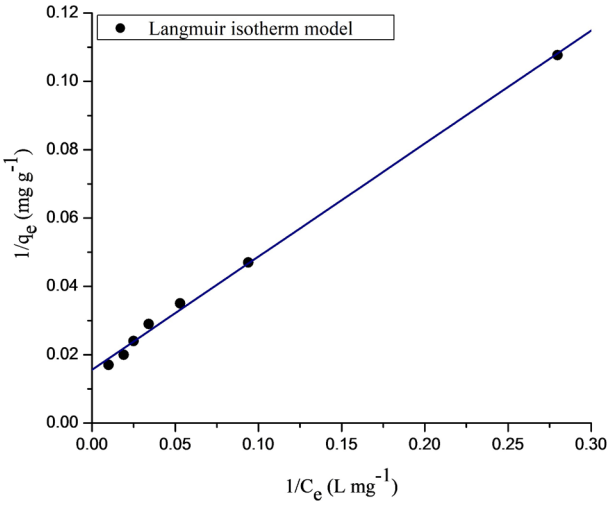

Fig. 9. Langmuir isotherm plot for CR dye adsorption by CAB immobilized with dual adsorbent (initial pH: 6; CR dye concentration: 50–400 mg L^{-1}; dual adsorbent loading in CAB: 4% (w/v); entrapped dual adsorbent dosage: 5 g L^{-1}; agitation speed: 180 rpm; temperature: 303 K; and contact time: 24 h).

Table 6
Adsorption isotherm model parameters for CR dye adsorption onto entrapped dual adsorbent

Isotherm	Model parameters	Values	Model equation
Freundlich	n	1.7009	$q_e = 4.6547C_e^{1.7}$
	K_F (L g^{-1})	4.6547	
	R^2	0.9811	
	χ^2	1.3302	
Langmuir	q_{max} (mg g^{-1})	64.0204	$q_e = \frac{3.022C_e}{1+0.0472C_e}$
	K_L (L mg^{-1})	0.0472	
	R^2	0.9987	
	χ^2	0.9687	
Temkin	K_T (L g^{-1})	0.3597	$q_e = 15.88\ln(0.36C_e)$
	b_T (kJ mol^{-1})	0.1586	
	R^2	0.9758	
	χ^2	8.9126	

surface of adsorbed layer is unimolecular [6,7]. The maximum monolayer adsorption capacity (q_{max}) and the Langmuir constant (K_L) were estimated as 64.02 mg g^{-1} and 0.0472 L mg^{-1}, respectively. The calculated R_L values at different initial dye concentration are shown in Fig. S5 of supplementary materials. From Fig. S5, it was observed that adsorption was found to be more favorable at higher concentrations. Also the value of the separation factor, R_L fell in the range of 0–1 at all initial dye concentration and this confirms the favorable uptake of the adsorption process [59]. Freundlich constant, n also varied from 1 to 10 which again proved that the adsorption is favorable. The q_{max} of the entrapped dual adsorbent for the removal of CR was compared with those of other adsorbents reported in the literature and the values are shown in Table 7. It can be inferred from Table 7 that the entrapped dual adsorbent has superior adsorption capacity compared with other adsorbents. The results revealed CAB immobilized with DB–WB dual adsorbent as a promising adsorbent for the removal of CR from aqueous solutions.

3.5. Effect of temperature and thermodynamic parameters

Various textile dye effluents are discharged at relatively high temperature (323–333 K); therefore, temperature can be an important parameter in the adsorption process for the real application of CAB immobilized with dual adsorbent. The effect of temperature on adsorption capacity (q_e) of entrapped dual adsorbent was studied by varying the temperature from 303 to 333 K and the results are shown in Fig. 10. From this figure, it is shown that the CR dye uptake (q_e) increased from 55.514 to 69.546 mg g^{-1} with the increase in temperature, suggests that the adsorption is an endothermic process. The maximum monolayer adsorption capacity, q_{max} of adsorbent increased from 64.02 mg g^{-1} at 303 K to 78.38 mg g^{-1} at 333 K, respectively. This is because the pore volume of the entrapped dual adsorbent particles was enlarged at elevated temperatures [74]. The pore volume was observed to increase from 0.8 mm^3 g^{-1} at room temperature (303 K) to 1.20 mm^3 g^{-1} at 333 K (Figs. S6 and S7). This phenomenon may be due to an increase in the mobility of CR dye molecules and reduces

Table 7
Comparison of maximum monolayer CR dye adsorption capacity of different adsorbents determined by Langmuir adsorption isotherm model

Adsorbent	Maximum adsorption capacity q_{max} (mg g^{-1})	Reference
Rubber seeds	9.82	[60]
Pineapple plant stem	11.97	[61]
Luffa cylindrica cellulosic fiber	17.39	[62]
Natural pumice	27.32	[63]
Fe–Zn bimetallic nanoparticles	28.56	[64]
Eucalyptus wood sawdust	31.25	[65]
Apricot stone activated carbon	32.85	[66]
Jute stick powder	35.70	[67]
Sugarcane bagasse	38.20	[68]
Neem leaf powder	41.24	[69]
Cross-linked cellulose dialdehyde	42.03	[70]
Jujuba seeds	55.56	[71]
Eichhonia charcoal	56.80	[72]
Phoenix dactylifera seeds	61.72	[73]
CAB immobilized with *Neurospora crassa* dead biomass–wheat bran	64.02	Present work

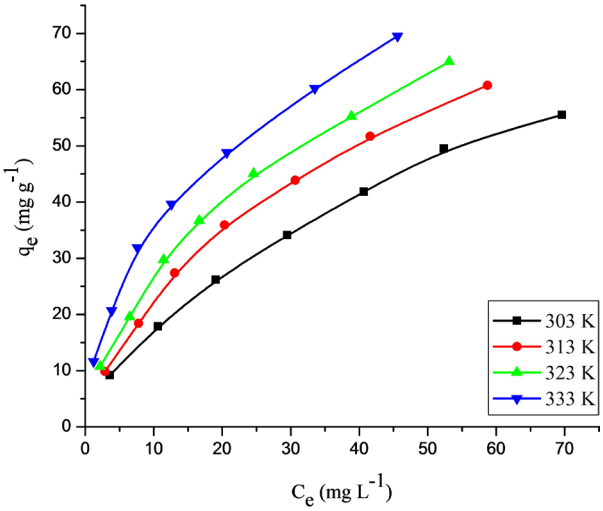

Fig. 10. Effect of temperature on CR dye adsorption by CAB immobilized with dual adsorbent (initial pH: 6; CR dye concentration: 50–400 mg L^{-1}; dual adsorbent loading in CAB: 4% (w/v); entrapped dual adsorbent dosage: 5 g L^{-1}; agitation speed: 180 rpm; and contact time: 24 h).

the swelling effect of it with increasing temperature [3]. An increasing number of dye molecules may also acquire sufficient energy to undergo an interaction with active sites at the

particle surface [75]. The enhancement in the adsorption capacity might be due to the chemical interaction between adsorbate and adsorbent or creation of some new adsorption active sites in the entrapped dual adsorbent particle surface [54].

The adsorption thermodynamics is useful to investigate whether the process is spontaneous or not and also to obtain an insight into the adsorption behavior. The thermodynamic parameters, such as change in Gibbs free energy (ΔG), change in enthalpy (ΔH), and change in entropy (ΔS) of the process for the adsorption of CR dye were determined using the following Eqs. (13)–(15) [74,75]:

$$\Delta G = -RT\ln(K_a) \tag{13}$$

$$\ln K_a = \frac{\Delta S_{ads}}{R} - \frac{\Delta H_{ads}}{RT} \tag{14}$$

$$K_a = q_{max} K_L \tag{15}$$

where K_a is the adsorption equilibrium constant (L g^{-1}). The thermodynamic parameters were calculated by plotting $\ln K_a$ vs. $1/T$ (Fig. 11), and the values are reported in Table 8. Table 8 shows that the values of ΔG decreased with the increase in temperature, suggesting that the adsorption

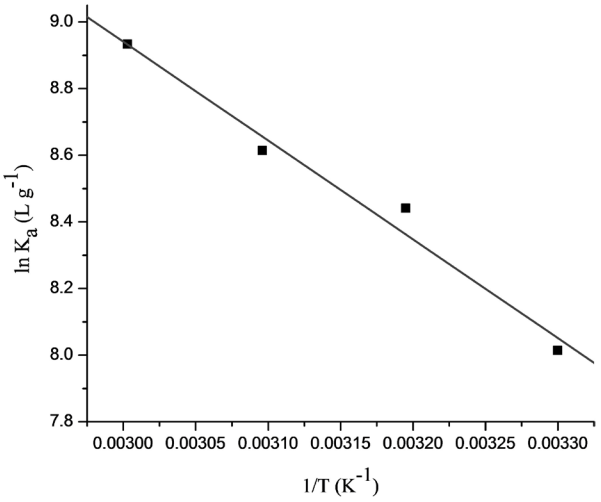

Fig. 11. Van't Hoff plot for CR dye adsorption by CAB immobilized with dual adsorbent (initial pH: 6; CR dye concentration: 50–400 mg L^{-1}; dual adsorbent loading in CAB: 4% (w/v); entrapped dual adsorbent dosage: 5 g L^{-1}; agitation speed: 180 rpm; temperature: 303–333 K; and contact time: 24 h).

was a spontaneous process. The values of ΔG become more negative with increasing temperature, demonstrating that higher temperature facilitates the adsorption of CR on CAB immobilized with dual adsorbent. The positive value of ΔH again proved that that the adsorption of CR onto the entrapped dual adsorbent was an endothermic process. The positive value of ΔS suggests increased randomness of dye molecules at the particle surface than in the dye solution.

The pseudo-second-order rate constant of CR dye adsorption on CAB immobilized with dual adsorbent is expressed as a function of temperature by the Arrhenius type relationship [72]:

$$\ln K_2 = \ln A - \left(\frac{E_a}{RT}\right) \tag{16}$$

where E_a is the activation energy of adsorption (kJ mol^{-1}), A is the Arrhenius frequency factor, and K_2 is the pseudo-second-order rate constant (g mg^{-1} min^{-1}) obtained for each reaction performed at 303–333 K with various concentration of dye solutions from 50 to 400 mg L^{-1}. The magnitude of activation energy gives an idea about the type of adsorption which is mainly physical or chemical. The physisorption processes usually have energies in the range 5–40 kJ mol^{-1} while higher activation energies (40–800 kJ mol^{-1}) suggest chemisorption [75,76]. An adsorption process is generally considered as physical if ΔH < 25 kJ mol^{-1} and as chemical when ΔH > 40 kJ mol^{-1} [77]. The activation energy of adsorption, determined from the slope of the linear plot of $\ln K_2$ vs. $1/T$ (Fig. 12), was found to be 23.89 kJ mol^{-1} with varying dye concentration from 50 to 400 mg L^{-1} (Table S1). The value of ΔH (24.66 kJ mol^{-1}) and activation energy (23.89 kJ mol^{-1}) indicates that CR adsorption onto the CAB immobilized with dual adsorbent is physical and endothermic reaction. This clearly revealed that the attractive force involved between the adsorbate and active sites in the entrapped dual adsorbent surface was not stronger.

3.6. Kinetic studies of adsorption

The rate of adsorption onto an entrapped dual adsorbent surface depends upon a number of parameters such as structural properties of adsorbent, initial concentrations of the solute, and the interaction between the solute and binding sites of the adsorbent [78]. Adsorption kinetics of CR dye using CAB immobilized with DB–WB dual adsorbent was carried out for different initial dye concentration ranging from 50 to 400 mg L^{-1}. To determine the rate constants of the adsorption process, the kinetics experimental

Table 8
Thermodynamic parameters for the adsorption of CR dye onto CAB immobilized with DB–WB dual adsorbent

Temperature (K)	Maximum adsorption capacity q_{max} (mg g^{-1})	Thermodynamic parameters		
		ΔG (kJ mol^{-1})	ΔH (kJ mol^{-1})	ΔS (kJ mol^{-1} K^{-1})
303	64.02	–20.187	24.656	0.148
313	67.74	–21.966		
323	72.56	–23.132		
333	78.38	–24.733		

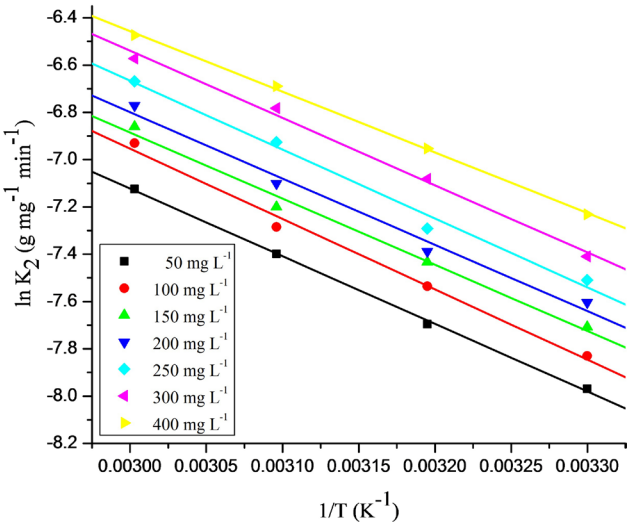

Fig. 12. Arrhenius plot for CR dye adsorption by CAB immobilized with dual adsorbent (initial pH: 6; CR dye concentration: 50–400 mg L^{-1}; dual adsorbent loading in CAB: 4% (w/v); entrapped dual adsorbent dosage: 5 g L^{-1}; agitation speed: 180 rpm; temperature: 303–333 K; and contact time: 24 h).

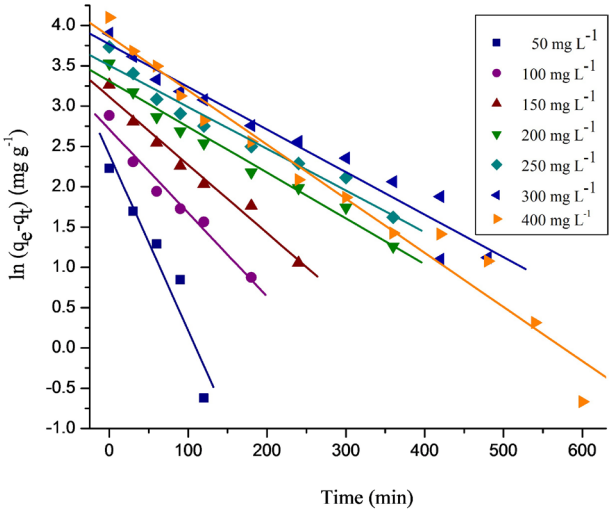

Fig. 13. Lagergren pseudo-first-order kinetic plot for CR dye adsorption by CAB immobilized with dual adsorbent (initial pH: 6; CR dye concentration: 50–400 mg L^{-1}; dual adsorbent loading in CAB: 4% (w/v); entrapped dual adsorbent dosage: 5 g L^{-1}; agitation speed: 180 rpm; temperature: 303 K; and contact time: 24 h).

data were simulated using Lagergren pseudo-first-order [79] and Ho's pseudo-second-order [13] kinetic models. The difference between the equilibrium solid phase concentration and solid phase concentration at time t is the driving force for adsorption, and the overall adsorption rate is proportional to either the driving force (as in pseudo-first-order equation) or the square of the driving force (as in pseudo-second-order equation) [80]. The linear forms of these two models are expressed by the following Eqs. (17) and (18) [13,79]:

Lagergren pseudo-first-order kinetic model:

$$\ln(q_e - q_t) = \ln q_e - K_1 t \tag{17}$$

where q_e is the amount of dye adsorbed from aqueous solution at equilibrium (mg g^{-1}), q_t is the amount of dye adsorbed on the adsorbent surface at any time t (min), and K_1 is the pseudo-first-order equilibrium rate constant (min^{-1}). The values of q_e and K_1 can be determined from the intercept and slope of the linear plot of $\ln(q_e - q_t)$ vs. t.

Ho's pseudo-second-order kinetic model:

$$\frac{t}{q_t} = \frac{1}{K_2 q_e^2} + \frac{t}{q_e} \tag{18}$$

where K_2 is the equilibrium rate constant of pseudo-second-order adsorption (g mg^{-1} min^{-1}). The straight line plot of t/q_t vs. t has been analyzed by linear regression to obtain the parameters of q_e and K_2. The correlation coefficient (R^2) calculated from these kinetic plots was used to evaluate the applicability of these models.

3.6.1. Inference from adsorption kinetic models

The adsorption of CR on CAB immobilized with dual adsorbent was not very rapid due to reduction of dye anion

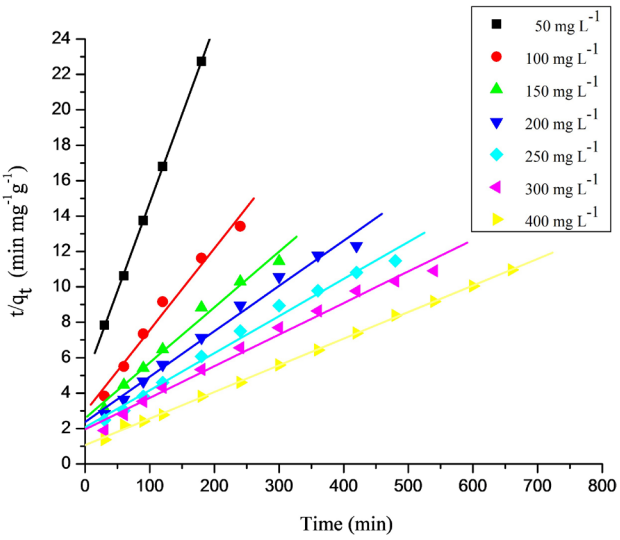

Fig. 14. Ho's pseudo-second-order kinetic plot for CR dye adsorption by CAB immobilized with dual adsorbent (initial pH: 6; CR dye concentration: 50–400 mg L^{-1}; dual adsorbent loading in CAB: 4% (w/v); entrapped dual adsorbent dosage: 5 g L^{-1}; agitation speed: 180 rpm; temperature: 303 K; and contact time: 24 h).

diffusion (slow diffusion) from aqueous phase. The pseudo-first-order and pseudo-second-order kinetic plots for CR dye adsorption were shown in Figs. 13 and 14, respectively, and the results of the kinetic parameters evaluated from these plots were given in Table 9. The linear regression coefficients, R^2 values (0.9953) for pseudo-second-order kinetic model at all the concentrations studied are higher than (close to 1) those for pseudo-first-order model. Also, the predicted q_e values obtained from pseudo-second-order kinetic model was closer and good agreement

Table 9
Kinetic parameters for the adsorption of CR dye onto CAB immobilized with DB–WB dual adsorbent

Initial dye concentration (mg L^{-1})	$q_{e,exp}$ (mg g^{-1})	Pseudo-first-order kinetic model				Pseudo-second-order kinetic model			
		$q_{e,cal}$ (mg g^{-1})	K_1 (min^{-1})	R^2	SD (%)	$q_{e,cal}$ (mg g^{-1})	K_2 (g mg^{-1} min^{-1})	R^2	SD (%)
50	9.285	10.995	0.0218	0.9563	7.52	10.009	2.098×10^{-3}	0.9999	3.18
100	17.880	15.068	0.0104	0.9643	6.42	18.654	7.258×10^{-4}	0.9912	1.77
150	26.193	22.542	0.0084	0.9782	5.69	26.888	3.815×10^{-4}	0.9924	0.47
200	34.104	27.387	0.0057	0.9824	8.04	35.063	2.764×10^{-4}	0.9943	1.15
250	41.871	33.307	0.0052	0.9803	8.35	42.355	2.120×10^{-4}	0.9969	1.08
300	49.530	43.269	0.0053	0.9754	9.16	50.054	1.634×10^{-4}	0.9928	0.43
400	60.273	47.797	0.0067	0.9835	8.45	60.489	2.141×10^{-4}	0.9996	1.24

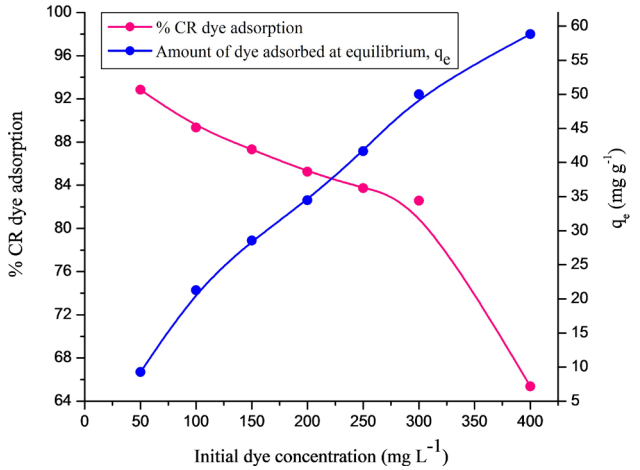

Fig. 15. Effect of initial dye concentration on CR dye adsorption by CAB immobilized with dual adsorbent (initial pH: 6; CR dye concentration: 50–400 mg L^{-1}; dual adsorbent loading in CAB: 4% (w/v); entrapped dual adsorbent dosage: 5 g L^{-1}; temperature: 303 K; and contact time: 24 h).

between experimental q_e values. It was suggested that the pseudo-second-order kinetic model is more suitable for adsorption of CR onto CAB immobilized with DB–WB dual adsorbent. The influence of dye concentration was analyzed by varying the initial dye concentration from 50 to 400 mg L^{-1}. The increase in dye concentration reduced the percentage adsorption of CR dye from 92.85% to 65.37% (Fig. 15). This is due to accumulation of solute molecules in the vacant sites and competition between more dye anions at the positive charge of fixed binding sites of the entrapped dual adsorbent. As the initial dye concentration was increased, the available binding sites on the surface of the entrapped dual adsorbent were saturated, leading to the decrease of the percentage adsorption (lack of available binding sites) [81]. The amount of dye adsorbed at equilibrium, q_e increased from 9.285 to 58.82 mg g^{-1} (Fig. 15) with increase in initial dye concentration from 50 to 400 mg L^{-1}. It can be proposed that an increase in initial dye concentration leads to an increase in concentration gradient between the adsorbate concentration in the solution and the surface of the entrapped dual adsorbent. This concentration gradient acts as a driving force for the transfer of dye molecules from bulk solution to the particle surface [49,82].

3.7. Validity of kinetic models

The adsorption kinetics of CR onto the prepared DB–WB dual adsorbent entrapped in CAB was verified at different initial dye concentrations. The validity of kinetic model was evaluated by the normalized standard deviation (SD, %), given by the following Eq. (19) [75]:

$$\mathrm{SD}(\%) = \sqrt{\left\{\frac{\sum\left[\frac{\left(q_{e,\mathrm{exp}} - q_{e,\mathrm{cal}}\right)}{q_{e,\mathrm{exp}}}\right]^2}{N_p - 1}\right\}} \times 100 \tag{19}$$

where N_p is the number of data points. The lower value of SD indicates the better fit of kinetic model. Table 9 lists the SD values obtained for the various kinetic models studied. It was found the pseudo-second-order kinetic model yielded the lowest SD values. This agrees with R^2 values (close to 1) obtained earlier and suggest that the adsorption of CR by CAB immobilized with dual adsorbent could be best described by the pseudo-second-order kinetic model.

3.8. Comparison of adsorption efficiency between calcium alginate blank beads and DB–WB dual adsorbent entrapped in CAB

The batch experiments for the adsorption of CR dye were carried out with calcium alginate blank beads and dual adsorbent entrapped in CAB in separate batches for the purpose of comparison. The initial CR dye concentration was fixed as 300 mg L^{-1} and was treated with 5 g L^{-1} of calcium alginate blank beads with an agitation speed of 180 rpm at 303 K. The percentage adsorption was calculated for regular time intervals and compared with the adsorption efficiency of the dual adsorbent entrapped in CAB (4% (w/v) loading of dual adsorbent in CAB with concentration of 5 g L^{-1}). The results were shown in Fig. 16. The CR adsorption by CAB (blank beads) was found to be 34.65%. But after immobilized with DB–WB dual adsorbent the adsorption efficiency increased to 82.56% (Table S2). It was observed that the CAB immobilized with dual adsorbent had better adsorption efficiency when compared with the calcium alginate blank beads.

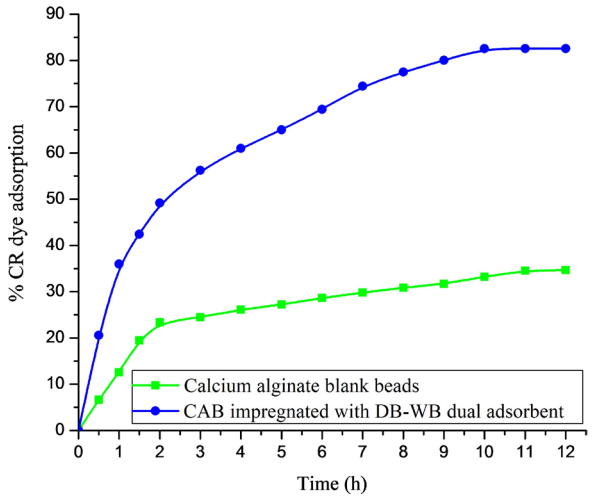

Fig. 16. Comparison of adsorption efficiency between calcium alginate blank beads and DB–WB dual adsorbent entrapped in CAB (initial pH: 6; CR dye concentration: 300 mg L^{-1}; dual adsorbent loading in CAB: 4% (w/v); entrapped dual adsorbent dosage: 5 g L^{-1}; calcium alginate (4% (w/v)) blank beads dosage: 0.5 g; agitation speed: 180 rpm; temperature: 303 K; and contact time: 12 h).

3.9. Desorption studies and reusability of the CAB immobilized with DB–WB dual adsorbent

The regeneration of adsorbent is important for the practical application of adsorption process. The adsorbent having regeneration ability is considered cost effective and applicable at industrial purposes. Stability is generally important when the same adsorbent is reused in multiple adsorption and desorption cycles. Therefore, the reusability of adsorbent was examined based on adsorption/desorption ability. Desorption experiments were conducted using various desorbing agents in separate batches to explore the possibility for recovery of entrapped dual adsorbent. The percentage of CR dye desorbed gradually decreased with an increasing number of runs. It was found that up to a maximum of 46.84% of the dye could be desorbed using the solvent methanol in the third run, compared with other desorbing agents (Table S3). This may be due to the low volume of the desorbing agent, which may prevent further release of bound dye anions to the solvent.

The regenerated entrapped dual adsorbent was added to the dye solution of concentration 300 mg L^{-1} with an agitation speed of 180 rpm at 303 K. The regenerated adsorbent was tested in the second and third runs. In comparison with the first run, 65.18% adsorption was maintained after 24 h in the second run and 54.72% in the third run (Table S4). This may be attributed to the incomplete desorption of the bound dye anions from the CAB immobilized with dual adsorbent surface (the immobilized dual adsorbent active site is almost blocked with CR dye molecules) and lack of binding sites on the entrapped particle surface. Therefore, the dye adsorption percentage gradually decreased in the subsequent runs.

4. Conclusion

The present study shows that the CAB immobilized with filamentous dead fungus *N. crassa*-wheat bran may be used as a potential adsorbent for the removal of CR dye from an aqueous solution. Additionally, the fungus was found to be free from pathogenicity. The various experimental factors, such as initial pH, dye concentration, dual adsorbent loading in CAB, adsorbent dosage, agitation speed, and temperature were optimized. A CCD was used to find the optimum process conditions with minimum number of experiments and these factors were found to be effective on the adsorption process. The CAB immobilized with dual adsorbent was characterized by ATR and FESEM/EDS techniques. The experimental data were analyzed using Freundlich, Langmuir, and Temkin isotherms models. The experimental equilibrium data were in good agreement with the Langmuir isotherm model. The maximum monolayer adsorption capacity (q_{max}) was 64.02 mg g^{-1} at 303 K. Thermodynamic parameters depicted the negative value of ΔG and the positive value of ΔH. This confirmed that the process is spontaneous and endothermic in nature and, thus, the adsorption is favorable at higher temperatures. The value of ΔH and activation energy clearly revealed that the adsorption of CR onto entrapped dual adsorbent is a physical process. The kinetic studies revealed that the adsorption process followed a pseudo-second-order rate equation. The maximum percentage of CR dye could be desorbed using the solvent methanol in desorption experiments. The regenerated entrapped dual adsorbent can be used up to three runs to adsorb CR dye in aqueous solutions without any loss of adsorbent or appreciable reduction in adsorption percentage. Comparison of adsorption efficiency between calcium alginate blank beads and CAB immobilized with dual adsorbent led to the observation that the entrapped dual adsorbent had better adsorption efficiency. The experimental results showed that the prepared immobilized material was a useful dual adsorbent for effective adsorption of anionic dyes from industrial effluents.

Symbols

A	—	Arrhenius frequency factor
Adj MS	—	Adjusted mean squares
Adj SS	—	Adjusted sum of squares
ANOVA	—	Analysis of variance
ATR	—	Attenuated transmission reflector
BET	—	Brunauer–Emmett–Teller
b_T	—	Adsorption energy, kJ mol^{-1}
CAB	—	Calcium alginate beads
CCD	—	Central composite design
CR	—	Congo red
C_o	—	Initial dye concentration in solution, mg L^{-1}
C_e	—	Equilibrium dye concentration in solution, mg L^{-1}
DB–WB	—	Dead biomass–wheat bran dual adsorbent
DF	—	Degrees of freedom
E_a	—	Activation energy of adsorption, kJ mol^{-1}
EDS	—	Energy dispersive X-ray spectroscopy
F	—	Fisher's F-test
f	—	Number of variables
FESEM	—	Field emission scanning electron microscopy
K_a	—	Adsorption equilibrium constant, L g^{-1}

K_F	—	Freundlich isotherm constant, L g^{-1}
K_L	—	Langmuir isotherm constant, L mg^{-1}
K_T	—	Temkin isotherm constant, L g^{-1}
K_1	—	Pseudo-first-order rate constant, min^{-1}
K_2	—	Pseudo-second-order rate constant, g mg^{-1} min^{-1}
MTCC	—	Microbial type culture collection
N	—	Numbers of experimental runs
N_P	—	Number of data points
N_o	—	Center points
n	—	Heterogeneity factor
P	—	Probability value
PRESS	—	Predicted residual error sum of squares
q_e	—	Amount of dye adsorbed at equilibrium, mg g^{-1}
$q_{e,\exp}$	—	Experimental adsorption capacity, mg g^{-1}
$q_{e,\text{cal}}$	—	Calculated adsorption capacity, mg g^{-1}
$q_{\max}$	—	Theoretical monolayer maximum saturation capacity, mg g^{-1}
q_t	—	Amount of dye adsorbed on the entrapped adsorbent surface at any time t, min
R	—	Universal gas constant, 8.314 J mol^{-1} K^{-1}
R^2	—	Linear regression correlation coefficient
R_L	—	Langmuir isotherm separation factor
S	—	Value of S chart
SD	—	Standard deviation
SE	—	Standard error
SEM	—	Scanning electron microscopy
Seq SS	—	Sequential sum of squares
$T_{\text{statistics}}$	—	Student's T-test
t	—	Adsorption time (min)
T	—	Temperature (K)
V	—	Volume of dye solution (mL)
W	—	Mass of dry CAB immobilized with DB–WB dual adsorbent, g.
x_i	—	Dimensionless value of a process variable X_i
X_i	—	Real value of an independent variable
X_o	—	Value of X_i at the center point
X_1	—	Initial pH
X_2	—	Initial dye concentration, mg L^{-1}
X_3	—	Entrapped dual adsorbent dosage, g
X_4	—	Agitation speed, rpm
Y	—	Predicted response variable of percentage adsorption
ΔG	—	Changes in Gibbs free energy, kJ mol^{-1}
ΔH	—	Changes in enthalpy, kJ mol^{-1}
ΔS	—	Changes in entropy, kJ mol^{-1} K^{-1}
2^f	—	Number of factorial points
$2f$	—	Axial points

Greek letters

β_o	—	Offset term
β_i	—	Regression coefficients for linear effect
β_{ii}	—	Regression coefficients for quadratic effect
β_{ij}	—	Regression coefficients for interaction effect
δX	—	Step change
χ^2	—	Chi-square test value

References

[1] A. Ozcan, E.M. Oncu, A. Safa Ozcan, Adsorption of acid blue 193 from aqueous solutions onto DEDMA-sepiolite, J. Hazard. Mater., 129 (2006) 244–252.

[2] R. Malarvizhi, N. Sulochana, Sorption isotherm and kinetic studies of methylene blue uptake onto activated carbon prepared from wood apple shell, J. Environ. Prot. Sci., 2 (2008) 40–46.

[3] V.S. Munagapati, D.S. Kim, Equilibrium isotherms, kinetics, and thermodynamics studies for congo red adsorption using calcium alginate beads impregnated with nano-goethite, Ecotoxicol. Environ. Saf., 141 (2017) 226–234.

[4] X.C. Jin, G.Q. Liu, Z.H. Xu, W.Y. Tao, Decolorization of a dye industry effluent by *Aspergillus fumigatus* XC6, Appl. Microbiol. Biotechnol., 74 (2007) 239–243.

[5] S.R. Couto, Dye removal by immobilized fungi, Biotechnol. Adv., 27 (2009) 227–235.

[6] W. Konicki, A. Hełminiak, W. Arabczyk, E. Mijowska, Removal of anionic dyes using magnetic Fe@graphite core-shell nanocomposite as an adsorbent from aqueous solutions, J. Colloid Interface Sci., 497 (2017) 155–164.

[7] V.S. Munagapati, D.S. Kim, Adsorption of anionic azo dye Congo Red from aqueous solution by cationic modified orange peel powder, J. Mol. Liq., 220 (2016) 540–548.

[8] H. Zhu, R. Jiang, J. Li, Y. Fu, S. Jiang, J. Yao, Magnetically recyclable Fe_3O_4/Bi_2S_3 microspheres for effective removal of Congo red dye by simultaneous adsorption and photocatalytic regeneration, Sep. Purif. Technol., 179 (2017) 184–193.

[9] Z.A. Medvedev, H.M. Crowne, M.N. Medvedeva, Age related variations of hepatocarcinogenic effect of azo dye (3'-MDAB) as linked to the level of hepatocyte polyploidization, Mech. Ageing Dev., **46 (1988) 159**–174.

[10] C. Srilakshmi, R. Saraf, Ag-doped hydroxyapatite as efficient adsorbent for removal of Congo red dye from aqueous solutions: synthesis, kinetic and equilibrium adsorption isotherm analysis, Microporous Mesoporous Mater., 219 (2016) 134–144.

[11] G. Crini, Non-conventional low cost adsorbents for dye removal: a review, Bioresour. Technol., 97 (2006) 1061–1085.

[12] A. Srinivasn, T. Viraraghavan, Decolorization of dye wastewaters by biosorbents: a review, J. Environ. Manage., 91 (2010) 1915–1929.

[13] Y.S. Ho, G. McKay, Pseudo-second order model for sorption processes, Process Biochem., 34 (1999) 451–465.

[14] J. Song, W. Zou, Y. Bian, F. Su, R. Han, Adsorption characteristics of methylene blue by peanut husk in batch and column modes, Desalination, 265 (2011) 119–125.

[15] T. Robinson, B. Chandran, P. Nigam, Removal of dyes from an artificial textile dye effluent by two agricultural waste residues, corncob and barley husk, Environ. Int., 28 (2002) 29–33.

[16] F. Ferrero, Dye removal by low cost adsorbents: hazelnut shells in comparison with wood sawdust, J. Hazard. Mater., 142 (2007) 144–152.

[17] B.H. Hameed, Evaluation of papaya seeds as a novel non-conventional low-cost adsorbent for removal of methylene blue, J. Hazard. Mater., 162 (2009) 939–944.

[18] X.S. Wang, J.P. Chen, Biosorption of congo red from aqueous solution using wheat bran and rice bran: batch studies, Sep. Sci. Technol., 44 (2009) 1452–1466.

[19] B.H. Hameed, Removal of cationic dye from aqueous solution using jackfruit peel as non-conventional low-cost adsorbent, J. Hazard. Mater., 162 (2009) 344–350.

[20] R. Gong, Y. Ding, M. Li, C. Yang, H. Liu, Y. Sun, Utilization of powdered peanut hull as biosorbent for removal of anionic dyes from aqueous solution, Dyes Pigm., 64 (2005) 187–192.

[21] B.E. Wang, Y. Hu, L. Xie, K. Peng, Biosorption behavior of azo dye by inactive CMC immobilized *Aspergillus fumigatus* beads, Bioresour. Technol., 99 (2008) 794–800.

[22] S.H. Chen, A.S. Ting, Biosorption and biodegradation potential of triphenylmethane dyes by newly discovered *Penicillium simplicissimum* isolated from indoor wastewater sample, Int. Biodeterior. Biodegrad., 103 (2015) 1–7.

[23] V. Prigione, G.C. Varese, L. Casieri, V.F. Marchisio, Biosorption of simulated dyed effluents by inactivated fungal biomasses, Bioresour. Technol., 99 (2008) 3559–3567.
[24] I. Kiran, T. Akar, S. Tunali, Biosorption of Pb(II) and Cu(II) from aqueous solutions by pretreated biomass of *Neurospora crassa*, Process Biochem.,40 (2005) 3550–3558.
[25] T. Akara, S. Arslanb, S.T. Akar, Utilization of *Thamnidium elegans* fungal culture in environmental cleanup: a reactive dye biosorption study, Ecol. Eng., 58 (2013) 363–370.
[26] T. Akar, A.S. Ozcan, S. Tunali, A. Ozcan, Biosorption of a textile dye (Acid Blue 40) by cone biomass of *Thuja orientalis*: estimation of equilibrium, thermodynamic and kinetic parameters, Bioresour. Technol., 99 (2008) 3057–3065.
[27] Z. Aksu, F. Gonen, Biosorption of phenol by immobilized activated sludge in a continuous packed bed: prediction of breakthrough curves, Process Biochem., 39 (2004) 599–613.
[28] R. Sudha Bai, T.E. Abraham, Studies on chromium(VI) adsorption–desorption using immobilized fungal biomass, Bioresour. Technol., 87 (2003) 17–26.
[29] N. Rangsayatorn, P. Pokethitiyook, E.S. Upatham, G.R. Lanza, Cadmium biosorption by cells of *Spirulina platensis* TISTR 8217 immobilized in alginate and silica gel, Environ. Int., 30 (2004) 57–63.
[30] L. Ai, M. Li, L. Li, Adsorption of methylene blue from aqueous solution with activated carbon/cobalt ferrite/alginate composite beads: kinetics, isotherms, and thermodynamics, J. Chem. Eng. Data, 56 (2011) 3475–3483.
[31] A.F. Hassan, A.M. Abdel-Mohsen, M.M.G. Fouda, Comparative study of calcium alginate, activated carbon, and their composite beads on methylene blue adsorption, Carbohydr. Polym., 102 (2014) 192–198.
[32] T.Y. Kim, H.J. Jin, S.S. Park, S.J. Kim, S.Y. Cho, Adsorption equilibrium of copper ion and phenol by powdered activated carbon, alginate bead and alginate-activated carbon bead, J. Ind. Eng. Chem., 14 (2008) 714–719.
[33] V. Rocher, J.M. Siaugue, V. Cabuil, A. Bee, Removal of organic dyes by magnetic alginate beads, Water Res., 42 (2008) 1290–1298.
[34] N.M. Mahmoodi, B. Hayati, M. Arami, H. Bahrami, Preparation, characterization and dye adsorption properties of biocompatible composite (alginate/titania nanoparticle), Desalination, 275 (2011) 93–101.
[35] P. Vairavel, V. Ramachandra Murty, S. Nethaji, Removal of Congo red dye from aqueous solutions by adsorption onto a dual adsorbent (*Neurospora crassa* dead biomass and wheat bran): optimization, isotherm, and kinetics studies, Desal. Wat. Treat., *68 (2017) 274–292*.
[36] A.A. Kadam, H.S. Lade, S.M. Patil, S.P. Govindwar, Low cost $CaCl_2$ pretreatment of sugarcane bagasse for enhancement of textile dyes adsorption and subsequent biodegradation of adsorbed dyes under solid state fermentation, Bioresour. Technol., 132 (2013) 276–284.
[37] R. Aravindhan, N.N. Fathima, J.R. Rao, B.U. Nair, Equilibrium and thermodynamic studies on the removal of basic black dye using calcium alginate beads, Colloids Surf., A, 299 (2007) 232–238.
[38] N. Saravanan, T. Kannadasan, C.A. Basha, V. Manivasagan, Biosorption of textile dye using immobilized bacterial (*Pseudomonas aeruginosa*) and fungal (*Phanerochate chrysosporium*) cells, Am. J. Environ. Sci., 9 (2013) 377–387.
[39] X. Han, W. Wang, X. Ma, Adsorption characteristics of methylene blue onto low cost biomass material lotus leaf, Chem. Eng. J., 171 (2011) 1–8.
[40] B. Zhang, X. Han, P. Gu, S. Fang, J. Bai, Response surface methodology approach for optimization of ciprofloxacin adsorption using activated carbon derived from the residue of desilicated rice husk, J. Mol. Liq., 238 (2017) 316–325.
[41] A. Asfaram, M. Ghaedi, S. Hajati, A. Goudarzi, A.A. Bazrafshan, Simultaneous ultrasound-assisted ternary adsorption of dyes onto copper-doped zinc sulfide nanoparticles loaded on activated carbon: optimization by response surface methodology, Spectrochim. Acta, 145 (2015) 203–212.
[42] K. Ravikumar, K. Pakshirajan, T. Swaminathan, K. Balu, Optimization of batch process parameters using response surface methodology for dye removal by a novel adsorbent, Chem. Eng. J., 105 (2005) 131–138.
[43] A. Sivasamy, S. Nethaji, J.L. Nisha, Equilibrium, kinetic and thermodynamic studies on the biosorption of reactive acid dye on *Enteromorpha flexuosa* and *Gracilaria corticata*, Environ. Sci. Pollut. Res., 19 (2012) 1687–1695.
[44] T. Robinson, B. Chandran, P. Nigam, Studies on desorption of individual textile dyes and a synthetic dye effluent from dye-adsorbed agricultural residues using solvents, Bioresour. Technol., 84 (2002) 299–301.
[45] A. Mittal, J. Mittal, A. Malviya, V.K. Gupta, Adsorptive removal of hazardous anionic dye "Congo red" from wastewater using waste materials and recovery by desorption, J. Colloid Interface Sci., 340 (2009) 16–26.
[46] B.H. Stuart, Infrared Spectroscopy: Fundamentals and Applications, John Wiley & Sons Ltd., New Jersey, United States (2004).
[47] M.C. Somasekhara Reddy, Removal of direct dye from aqueous solutions with an adsorbent made from tamarind fruit shell, an agricultural solid waste, J. Sci. Ind. Res., 65 (2006) 443–446.
[48] M. Spinti, H. Zhuang, E.M. Trujillo, Evaluation of immobilized biomass beads for removing heavy metals from wastewaters, Water Environ. Res., 67 (1995) 943–952.
[49] V. Vadivelan, K. Vasanth Kumar, Equilibrium, kinetics, mechanism, and process design for the sorption of methylene blue onto rice husk, J. Colloid Interface Sci., 286 (2005) 90–100.
[50] G. Crini, H.N. Peindy, F. Gimbert, C. Robert, Removal of C.I. basic green 4 (malachite green) from aqueous solutions by adsorption using cyclodextrin-based adsorbent: kinetic and equilibrium studies, Sep. Purif. Technol., 53 (2007) 97–110.
[51] K.K. Wong, C.K. Lee, K.S. Low, M.J. Haron, Removal of Cu and Pb by tartaric acid modified rice husk from aqueous solutions, Chemosphere, 50 (2003) 23–28.
[52] E. Errais, J. Duplay, F. Darragi, I.M. Rabet, A. Aubert, F. Huber, G. Morvan, Efficient anionic dye adsorption on natural untreated clay: kinetic study and thermodynamic parameters, Desalination, 275 (2011) 74–81.
[53] M.B. Kasiri, A.R. Khataee, Photooxidative decolorization of two organic dyes with different chemical structures by UV/H_2O_2 process: experimental design, Desalination, 270 (2011) 151–159.
[54] I.A.W. Tan, B.H. Hameed, A.L. Ahmad, Equilibrium and kinetic studies on basic dye adsorption by oil palm fibre activated carbon, Chem. Eng. J., 127 (2007) 111–119.
[55] H.M.F. Freundlich, Over the adsorption in solution, J. Phys. Chem., 385 (1906) 385–470.
[56] I. Langmuir, The adsorption of gases on plane surfaces of glass, mica and platinum, J. Am. Chem. Soc., 40 (1918) 1361–1403.
[57] K.R. Hall, L.C. Eagleton, A. Acrivos, T. Vermeulen, Pore and solid diffusion kinetics in fixed-bed adsorption under constant pattern conditions, Ind. Eng. Chem. Fundam., 5 (1966) 212–223.
[58] M.J. Temkin, V. Pyzhev, Kinetics of ammonia synthesis on promoted iron catalysts, Acta Physicochim. U.R.S.S., 12 (1940) 217–222.
[59] S. Nethaji, A. Sivasamy, G. Thennarasu, S. Saravanan, Adsorption of malachite green dye onto activated carbon derived from *Borassus aethiopum* flower biomass, J. Hazard. Mater., 181 (2010) 271–280.
[60] M.A. Zulfikar, H. Setiyanto, Rusnadi, L. Solakhudin, Rubber seeds (*Hevea brasiliensis*): an adsorbent for adsorption of Congo red from aqueous solution, Desal. Wat. Treat., 56 (2015) 2976–2987.
[61] S.L. Chan, Y.P. Tan, A.H. Abdullah, S.T. Ong, Equilibrium, kinetic and thermodynamic studies of a new potential biosorbent for the removal of Basic Blue 3 and Congo Red dyes: pineapple (*Ananas comosus*) plant stem, J. Taiwan Inst. Chem. Eng., 61 (2016) 306–315.
[62] V.K. Gupta, D. Pathania, S. Agarwal, S. Sharma, Amputation of congo red dye from waste water using microwave induced grafted *Luffa cylindrica* cellulosic fiber, Carbohydr. Polym., 111 (2014) 556–566.
[63] H. Shayesteh, A.R. Kelishami, R. Norouzbeigi, Evaluation of natural and cationic surfactant modified pumice for congo red removal in batch mode: kinetic, equilibrium, and thermodynamic studies, J. Mol. Liq., 221 (2016) 1–11.

[64] R.K. Gautam, V. Rawat, S. Banerjee, M.A. Sanroman, S. Soni, S.K. Singh, M.C. Chattopadhyaya, Synthesis of bimetallic Fe–Zn nanoparticles and its application towards adsorptive removal of carcinogenic dye malachite green and Congo red in water, J. Mol. Liq., 212 (2015) 227–236.
[65] V.S. Mane, P.V. Vijay Babu, Kinetic and equilibrium studies on the removal of Congo red from aqueous solution using Eucalyptus wood (*Eucalyptus globulus*) saw dust, J. Taiwan Inst. Chem. Eng., 44 (2013) 81–88.
[66] M. Abbas, M. Trari, Kinetic, equilibrium and thermodynamic study on the removal of Congo Red from aqueous solutions by adsorption onto apricot stone, Process Saf. Environ. Prot., 98 (2015) 424–436.
[67] G.C. Panda, S.K. Das, A.K. Guha, Jute stick powder as a potential biomass for the removal of congo red and rhodamine B from their aqueous solution, J. Hazard. Mater., 164 (2009) 374–379.
[68] Z. Zhang, L. Moghaddam, I.M. O'Hara, W.O.S. Doherty, Congo red adsorption by ball-milled sugarcane bagasse, Chem. Eng. J., 178 (2011) 122–128.
[69] K.G. Bhattacharyya, S. Arunima, *Azadirachta indica* leaf powder as an effective biosorbent for dyes: a case study with aqueous Congo Red solutions, J. Environ. Manage., 71 (2004) 217–229.
[70] S. Kumari, D. Mankotia, G.S. Chauhan, Crosslinked cellulose dialdehyde for Congo red removal from its aqueous solutions, J. Environ. Chem. Eng., 4 (2016) 1126–1136.
[71] M.C.S. Reddy, L. Sivaramakrishna, A.V. Reddy, The use of an agricultural waste material, Jujuba seeds for the removal of anionic dye (Congo red) from aqueous medium, J. Hazard. Mater., 203–204 (2012) 118–127.
[72] S. Kaur, S. Rani, R.K. Mahajan, Adsorption kinetics for the removal of hazardous dye Congo red by biowaste materials as adsorbents, J. Chem., 2013 (2013) 1–12.
[73] D. Pathania, A. Sharma, Z.M. Siddiqi, Removal of congo red dye from aqueous system using *Phoenix dactylifera* seeds, J. Mol. Liq., 219 (2016) 359–367.
[74] M.T. Sulak, E. Demirbas, M. Kobya, Removal of astrazon yellow 7GL from aqueous solutions by adsorption onto wheat bran, Bioresour. Technol., 98 (2007) 2590–2598.
[75] B.H. Hameed, A.A. Ahmad, N. Aziz, Isotherms, kinetics and thermodynamics of acid dye adsorption on activated palm ash, Chem. Eng. J., 133 (2007) 195–203.
[76] L. Abramian, H. EI-Rassy, Adsorption kinetics and thermodynamics of azo-dye orange II onto highly titania aerogel, Chem. Eng. J., 150 (2009) 403–410.
[77] V.K. Gupta, D. Pathania, S. Sharma, S. Agarwal, P. Singh, Remediation and recovery of methyl orange from aqueous solution onto acrylic acid grafted *Ficus carica* fiber: isotherms, kinetics and thermodynamics, J. Mol. Liq., 177 (2013) 325–334.
[78] R. Elangovan, L. Philip, K. Chandraraj, Biosorption of hexavalent and trivalent chromium by palm flower (*Borassus aethiopum*), Chem. Eng. J., 141 (2008) 99–111.
[79] S. Lagergren, Zur theorie der sogenannten adsorption geloster stoffe, K. Sven. Vetensk.akad. Handl., 24 (1898) 1–39.
[80] Z. Wu, H. Joo, K. Lee, Kinetics and thermodynamics of the organic dye adsorption on the mesoporous hybrid xerogel, Chem. Eng. J., 112 (2005) 227–236.
[81] N.K. Amin, Removal of reactive dye from aqueous solutions by adsorption onto activated carbons prepared from sugarcane bagasse pith, Desalination, 223 (2008) 152–161.
[82] B. Meroufel, O. Benali, M. Benyahia, Y. Benmoussa, M.A. Zenasni, Adsorptive removal of anionic dye from aqueous solutions by Algerian kaolin: characteristics, isotherm, kinetic and thermodynamic studies, J. Mater. Environ. Sci., 4 (2013) 482–491.

Supplementary materials

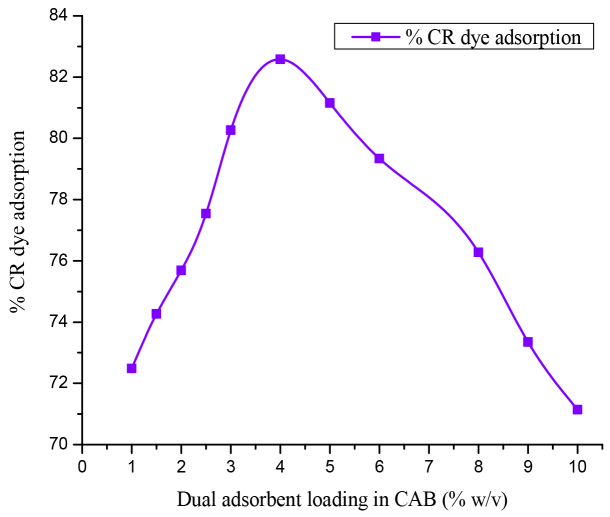

Fig. S1. Effect of dual adsorbent loading in CAB on CR dye adsorption (initial pH: 6; initial dye concentration: 300 mg L^{-1}; entrapped dual adsorbent dosage: 5 g L^{-1}; agitation speed: 180 rpm; temperature: 303 K; and contact time 10 h).

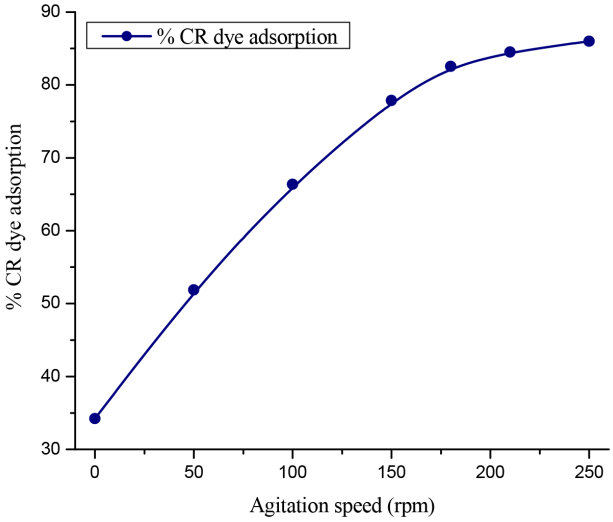

Fig. S3. Effect of agitation speed on CR dye adsorption by CAB immobilized with dual adsorbent (initial pH: 6; initial dye concentration: 300 mg L^{-1}; dual adsorbent loading in CAB: 4% (w/v); entrapped dual adsorbent dosage: 5 g L^{-1}; temperature: 303 K; and contact time: 10 h).

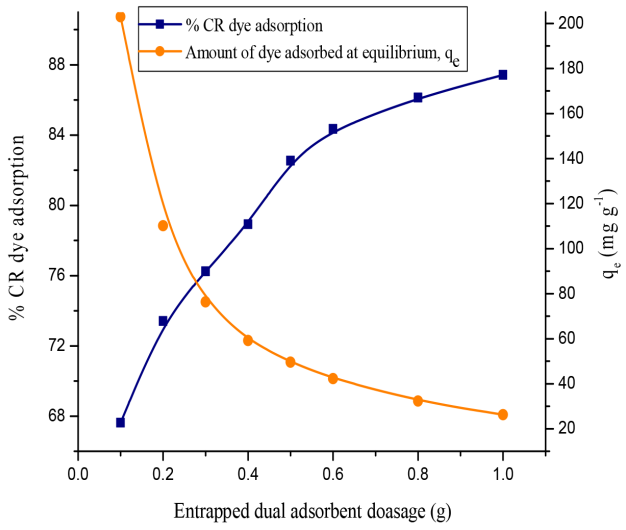

Fig. S2. Effect of entrapped dual adsorbent dosage on CR dye adsorption (initial pH: 6; initial dye concentration: 300 mg L^{-1}; dual adsorbent loading in CAB: 4% (w/v); agitation speed: 180 rpm; temperature: 303 K; contact time 10 h; and volume of dye solution: 100 mL).

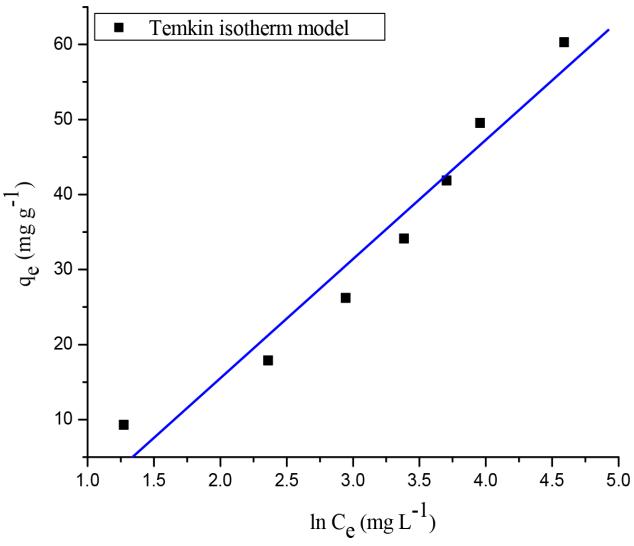

Fig. S4. Temkin isotherm plot for CR dye adsorption by CAB immobilized with dual adsorbent (initial pH: 6; CR dye concentration: 50–400 mg L^{-1}; dual adsorbent loading in CAB: 4% (w/v); entrapped dual adsorbent dosage: 5 g L^{-1}; agitation speed: 180 rpm; temperature: 303 K; and contact time: 24 h).

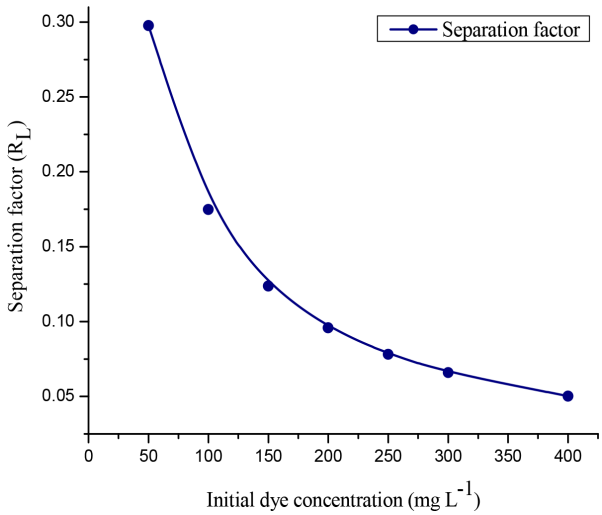

Fig. S5. Separation factor for CR dye adsorption by CAB immobilized with dual adsorbent (initial pH: 6; CR dye concentration: 50–400 mg L^{-1}; dual adsorbent loading in CAB: 4% (w/v); entrapped dual adsorbent dosage: 5 g L^{-1}; agitation speed: 180 rpm; temperature: 303 K; and contact time: 24 h).

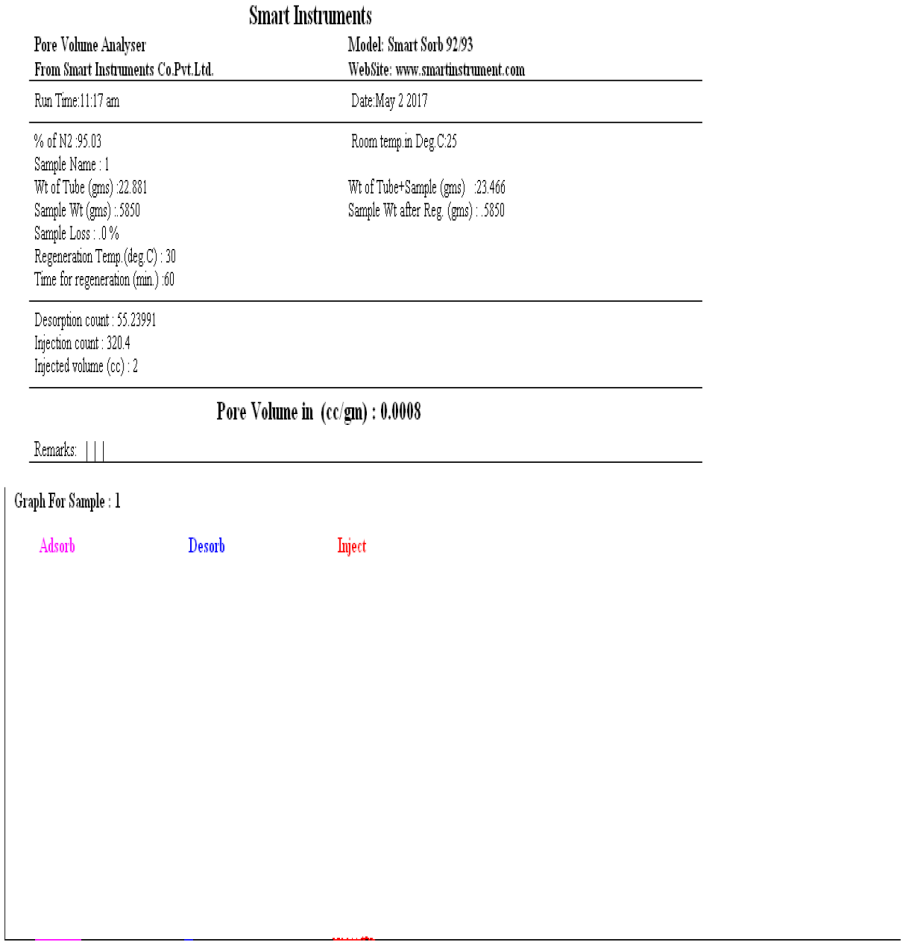
Smart Instruments

Pore Volume Analyser	Model: Smart Sorb 92/93
From Smart Instruments Co.Pvt.Ltd.	WebSite: www.smartinstrument.com
Run Time:11:17 am	Date:May 2 2017
% of N2 :95.03	Room temp.in Deg.C:25
Sample Name : 1	
Wt of Tube (gms) :22.881	Wt of Tube+Sample (gms) :23.466
Sample Wt (gms) : .5850	Sample Wt after Reg. (gms) : .5850
Sample Loss : .0 %	
Regeneration Temp.(deg.C) : 30	
Time for regeneration (min.) :60	
Desorption count : 55.23991	
Injection count : 320.4	
Injected volume (cc) : 2	

Pore Volume in (cc/gm) : 0.0008

Remarks: | | |

Fig. S6. Pore volume of CAB immobilized with dual adsorbent at 303 K.

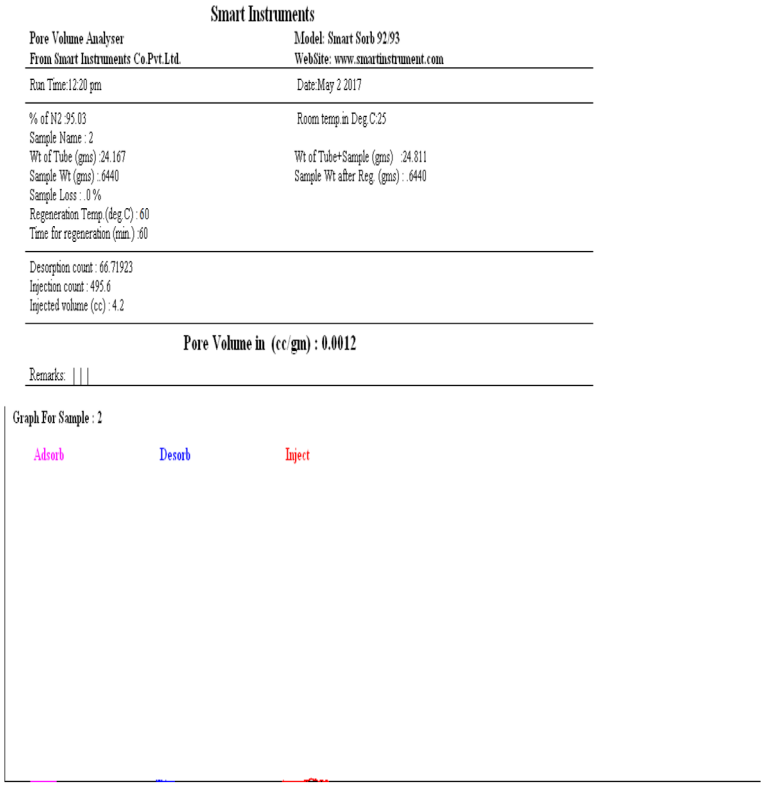

Fig. S7. Pore volume of CAB immobilized with dual adsorbent at 333 K.

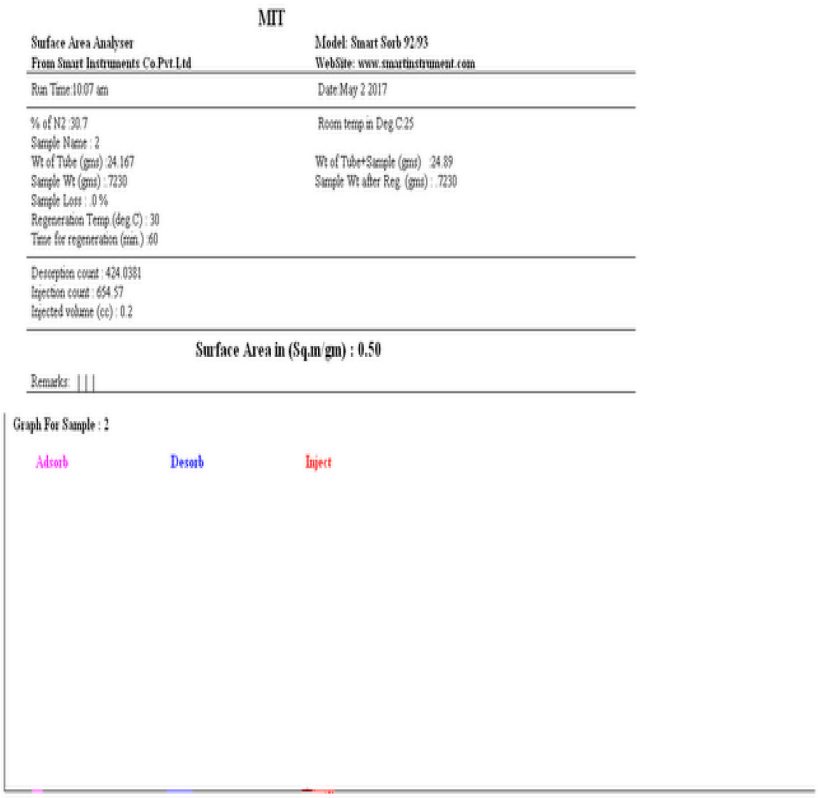

Fig. S8. BET surface area of CAB immobilized with 4% (w/v) DB–WB dual adsorbent at 303 K.

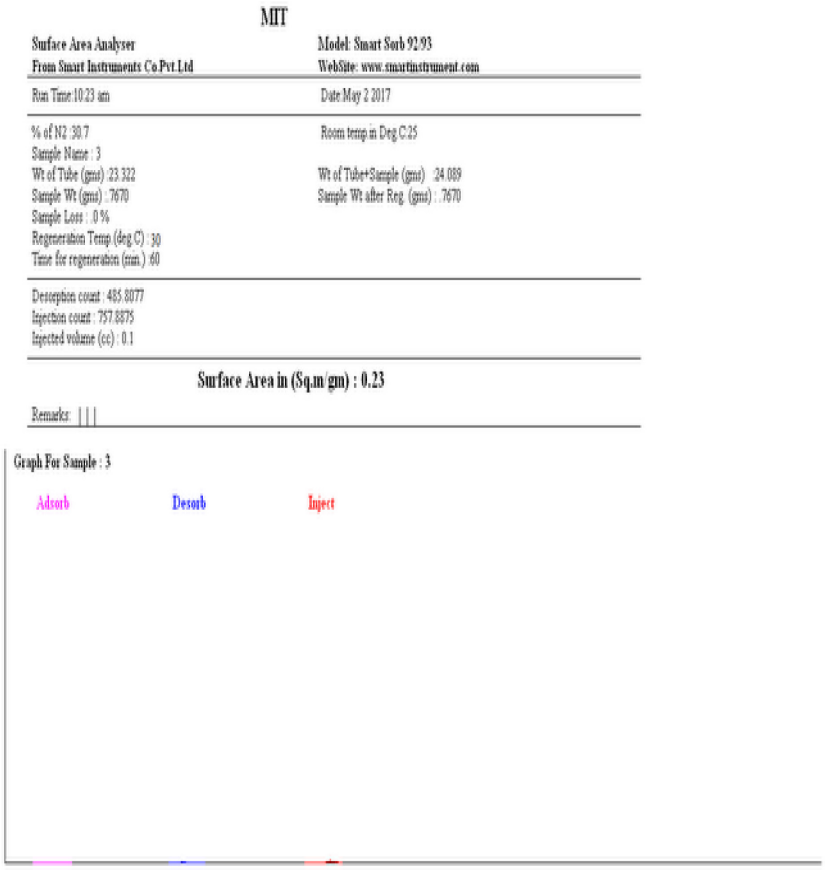

Fig. S9. BET surface area of CAB immobilized with 10% (w/v) DB–WB dual adsorbent at 303 K.

Table S1
Activation energy for the adsorption of CR dye onto CAB immobilized with DB–WB dual adsorbent at various dye concentrations

Initial dye concentration (mg L^{-1})	Activation energy, E_a (kJ mol^{-1})
50	23.778
100	24.712
150	23.244
200	23.308
250	24.211
300	23.644
400	24.316

Table S2
Comparison of adsorption efficiency between calcium alginate blank beads and DB–WB dual adsorbent entrapped in CAB

Time (h)	% adsorption of CR dye	
	Calcium alginate blank beads	CAB immobilized with dual adsorbent
0	0	0
0.5	6.64	20.56
1	12.56	35.98
1.5	19.49	42.44
2	23.35	49.19
3	24.47	56.25
4	26.13	61.02
5	27.24	64.99
6	28.67	69.44
7	29.79	74.45
8	30.84	77.52
9	31.73	80.13
10	33.25	82.56
11	34.54	82.56
12	34.65	82.56

Table S3
Desorption studies for the removal of CR dye from the entrapped dual adsorbent in various runs

S.No.	Desorbing agent	% desorption of CR dye from the entrapped dual adsorbent		
		First run	Second run	Third run
1	Methanol	73.56	60.48	46.84
2	Ethanol	49.47	35.62	18.53
3	Isopropyl alcohol	26.75	15.42	6.38
4	Butanol	21.60	10.24	4.65
5	1 M NaOH	68.12	52.76	40.38
6	Acetone	35.33	20.62	11.56

Note: Volume of desorbing agent: 100 mL; agitation speed: 180 rpm; temperature: 303 K; and contact time: 24 h.

Table S4
Reusability of CAB immobilized with DB–WB dual adsorbent for the adsorption of CR dye in various runs

S.No.	Desorbing agent	% adsorption of CR dye by regenerated entrapped dual adsorbent		
		First run	Second run	Third run
1	Methanol	82.58	65.18	54.72
2	Ethanol	82.52	45.56	32.84
3	Isopropyl alcohol	82.56	24.25	17.92
4	Butanol	82.53	18.44	8.65
5	1 M NaOH	82.56	58.74	46.34
6	Acetone	82.58	39.34	27.18

Note: pH: 6; initial dye concentration: 300 mg L^{-1}; agitation speed: 180 rpm; temperature: 303 K; and contact time: 24 h.